TECHNISCHE UNIVERSITÄT WIEN
Vienna | Austria

ATOMINSTITUT

Diplomarbeit

Reduction Of Reactor Pressure Vessel Activation Through Neutron Capture In The Biological Shield

zur Erlangung des akademischen Grades

Diplom-Ingenieur

im Rahmen des Studiums

Physikalische Energie- und Messtechnik

eingereicht von

Christoph Weindl
Matrikelnummer 01154791

ausgeführt am Atominstitut
der Fakultät für Physik der Technischen Universität Wien

Betreuung
Betreuer: Ao.Univ.Prof.i.R. Dr. Helmuth Böck
Dipl.-Ing. Dr.techn. Mario Villa
Mitwirkung: Dipl.-Ing. Dr.techn. Sam Karimzadeh

Wien, 29.04.2019

Unterschrift Verfasser

Unterschrift Betreuer

Danksagung

Ich möchte mich bei Herrn Prof. Dr. Helmuth Böck für seine großartige Unterstützung, nicht nur im Zuge dieser Diplomarbeit, sondern während meines gesamten Studiums, bedanken. Dr. Sam Karimzadeh danke ich für seine unschätzbare Hilfe bei der Entstehung dieser Arbeit.

An dieser Stelle möchte ich mich außerdem aufrichtig bei meiner Familie und meinen Freunden für ihre fortwährende Unterstützung und Motivation bedanken.

Abstract

Future dismantling of a nuclear power plant is doubtlessly a prime aspect, not only for manufacturers and customers, but also for society as a whole when it comes to the peaceful use of nuclear power. The three variants of Decontamination and Decommissioning are DECON, with a dismantling time up to 10 years, SAFSTOR, with a dismantling time of 50 to 60 years, and ENTOMB, which features permanent enclosure. This is to allow built-up radionuclides to decay so that the working environment is safe. Shortening the time-frame for decommissioning of a nuclear power plant would not only lead to financial and logistical advantages, but also to greater public acceptance of nuclear power.

This paper focuses on the activation of the reactor pressure vessel (RPV) in a pressurized water reactor. This activation is partially a result of fast neutrons which exit the reactor core, transmit through the RPV, get thermalized in the Biological Shield (BioS), diffuse back to the outer RPV wall and there activate different trace elements in the steel and plating. This paper will focus on evaluation of the attenuating effects of seeding the BioS with neutron absorbing materials, such as boron, and adding absorbing covers to the BioS.

Kurzfassung

Der zukünftige Abbau von Kernkraftwerken ist zweifelsohne ein wichtiger Aspekt der friedlichen Nutzung der Kernenergie, nicht nur für Hersteller und Betreiber, sondern für die gesamte Gesellschaft. Die drei etablierten Varianten zur Dekontaminierung und Stilllegung sind DECON, mit einem Rückbauzeitrahmen von bis zu 10 Jahren, SAFSTOR, mit einem Zeitrahmen von 50 bis 60 Jahren, und ENTOMB, dem dauerhaften Einschluss. Diese Maßnahmen gewährleisten einen Zerfall der aufgebauten Radionuklide auf ein Maß, welches ein sicheres Arbeitsumfeld für Rückbaumaßnahmen garantiert. Die Verkürzung dieser Zeiträume würde nicht nur finanzielle und logistische Vorteile bieten, sondern auch helfen, die gesellschaftliche Akzeptanz gegenüber der Kernenergie zu erhöhen.
Diese Arbeit befasst sich mit der Aktivierung des Reaktordruckbehälters (RDB) in einem Druckwasserreaktor. Diese Aktivierung ist zum Teil ein Resultat von schnellen Neutronen, welche den Reaktorkern verlassen, durch den RDB transmittieren, im biologischen Schild moderiert werden, zurück zur Außenwand des Druckbehälters diffundieren und dort Spurenelemente im Stahl und der Plattierung aktivieren. Diese Arbeit konzentriert sich auf die Evaluierung der Reduktion dieses Effekts durch Beifügung von neutronenabsorbierenden Materialien, wie zum Beispiel Bor, in das biologische Schild und der Anbringung von absorbierenden Abdeckungen am biologischen Schild.

Contents

List of Figures

1. Introduction

The decommissioning and dismantling of a nuclear power plant generally creates a number of challenges that make such a venture a lengthy process which can extend over decades. The main reason for this is the necessary professional handling of radioactive materials. On one hand, the focus of dismantling is, of course, on reducing or avoiding radiation exposure of the personnel deployed, but also on reducing the amount of waste, reusing materials and eventually reducing the associated costs.

In this respect, decommissioning of a nuclear power plant basically offers two strategies, as defined by the Nuclear Energy Institute [1]:

- DECON
- SAFSTOR

With DECON the emphasis is placed on decontamination and disassembly with a subsequent transfer to appropriate deposits soon after the facility closes. The challenge with this concept is the necessary radiation protection effort. Work on plant parts in which decontamination is not or only conditionally applicable, e.g. pressure vessel, are generally performed underwater using remote-controlled systems.
The aim of this prcedure is the use of exisiting infrastructure at the power plant site, as well as own and third-party personnel, which has the necessary knowledge about the system to reduce time and ultimately costs of dismantling.
The DECON process usually seeks for a dismantling time of up to ten years.

The SAFSTOR approach, in turn, is scheduled for a dismantling time of 50 to 60 years. The power plant is placed in a condition in which the amount of radioactive substances formed is allowed to reduce by natural decay. The main components of the power plant, such as the RPV, remain in place. The period of 50 to 60 years on one hand is mainly determined by the isotope ^{60}Co, which accounts for a large part of the "short-lived" radiation exposure. The half-life of ^{60}Co is 5.27 years, which means that after ten half-lives, or around 50 years, its activity has fallen to about one one-thousandth. Thereafter, the radiation load is the result of long-lived isotopes, such as ^{94}Nb with a half-life of about 20,000 years, which is why a longer waiting period would not make sense. Furthermore,

as required by the NRC, decommissioning must be completed within 60 years of the plant ceasing operation. [1]
Whilst the necessary radiation protection effort for this procedure is reduced compared to DECON, the financial burden with SAFSTOR is greater: new staff must be hired after the waiting period has elapsed, the safety of the facility must be guaranteed at all times and general public acceptance for this strategy is low.

Another option for decommissioning is the ENTOMB process, i.e. the permanent enclosure of contaminated or activated power plant components. However, this procedure has not been used to this day.

One major component in the decommissioning and dismantling process is the reactor pressure vessel. Fig. 1 shows the neutron flux contour in the area of the pressure vessel in the radial direction. It can be clearly seen that the profile has its maximum at the inside of the RPV and then decreases. After about two thirds of the RPV, the profile has a minimum and then increases again towards the outer wall. [2]

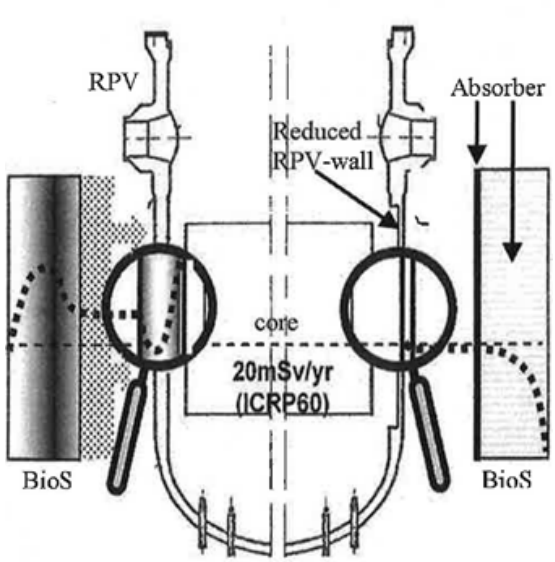

Fig. 1: Neutron flux contour [3]

This increase of the thermal neutron flux towards the outer boundary of the reactor pressure vessel is caused by the following phenomenon: fast and epithermal neutrons, which

are part of the reactors neutron spectrum, exit the core and penetrate the reactor pressure vessel, because of their low interaction probability. These neutron then enter the Biological Shield, which is placed to reduce the effects of ionizing radiation outside of the reactor and also to support the reactor itself. Because of its composition, the BioS has relatively good moderation qualities, which results in the built-up of thermal neutrons in the BioS. These thermal neutrons then diffuse back towards the RPV, where they are subsequently absorbed. This absorption causes activation of different trace elements in the RPV steel. These activated elements are generally radioactive and eventually cause increased dose rates at the outer side of the RPV. In order to reduce the activation of the outer RPV layers, one would have to decrease the thermal neutron flux originating from the BioS. In this thesis, two approaches for achieving this reduction will be discussed: boron-doping the BioS and adding cadmium cladding to the BioS.

The following chapters will describe theoretical aspects necessary for this thesis, take a closer look at reactor design and will describe the applied calculation methods as well as their results. A summary will be given at the end.

2. Theoretical Principles

The following subchapters address the necessary physical fundamentals and principles, which are necessary for this thesis. These are radioactivity in general, neutron physics and nuclear fission. A description of the basics of neutron transport and Monte-Carlo simulation, which was used for this thesis, is given in Chapter 4.

2.1 Radioactivity

Radioactivity describes the process by which unstable nuclei dissipate excess energy by particle and/or gamma ray emission. While particle radiation, i.e. alpha, beta and neutron radiation, results in the conversion into other nuclei, gamma ray emission does not change the emitting nucleus.
In the following, the different types of radiation are explained in more detail.

2.1.1 Alpha radiation

Alpha radiation describes the emission of a double positively charged helium nucleus. This means that the parent nucleus loses two protons and two neutrons.

$$ {}^{A}_{Z}X \rightarrow {}^{A-4}_{Z-2}Y + {}^{4}_{2}He + \Delta E \tag{2.1} $$

Alpha decay is a two-body problem, which results in a discrete energy distribution. However, since the energy ΔE released by the mass defect either completely goes into kinetic energy of the decay products or can remain in the daughter nucleus as excitation energy, which is later emitted as gamma radiation, several energy lines can occur for one isotope. Furthermore, the released energy ΔE depends on whether the parent nucleus was in an excited or in the ground state prior to decay.

Due to the positive charge and relative large mass of the alpha particle, it strongly interacts with matter, resulting in a low penetration depth. The biological effect of alpha radiation on the human body from the outside is comparatively low, but inhalation or incorporation can lead to considerable damage.

2.1.2 Beta radiation

Beta radiation is the most common type of radioactive decay. Like alpha radiation, beta radiation is also a form of particle radiation. A distinction is made between two basic types of beta radiation: beta plus and beta minus decay.

Beta-plus radiation describes the decay of a proton into a neutron, a positron and an electron neutrino, the latter two leaving the nucleus.

$$ {}^{A}_{Z}X \rightarrow {}_{Z-1}{}^{A}Y + e^{+} + \nu \tag{2.2} $$

This decay occurs in nuclides with excess protons. The atomic number is reduced by one while the mass number remains the same.

By contrast, beta-minus radiation describes the decay of a neutron into a proton, an electron and an electron antineutrino, with the latter two leaving the nucleus.

$$ {}^{A}_{Z}X \rightarrow {}_{Z+1}{}^{A}Y + e^{-} + \overline{\nu} \tag{2.3} $$

This decay occurs in nuclides with excess neutrons. The atomic number is increased by one, while the mass number remains the same.

Since this is a three-body-decay, unlike alpha decay, there is no discrete but a continuous energy distribution.

Due to the lower charge and mass of the electron or positron, the range is greater than with alpha radiation. For example, beta particles can penetrate skin and cause severe burns. Inhalation and incorporation, as with alpha radiation, can also cause significant damage, but the affected environment is larger than with inhaled or incorporated alpha emitters. Furthermore, as being the antiparticle of the electron, after dissipating its kinetic energy, the positron will eventually recombine with an electron. This annihilation process results in the emission of two 511 keV photons and has also be taken into account radiologically.

2.1.3 Gamma radiation

Gamma radiation describes electromagnetic radiation with energies above 100 keV. Gamma decay usually takes place as a concomitant to alpha and beta decay, which leave the newly formed nucleus in excited rotational and/or vibrational states. This excitation energy can then be emitted in the form of one or more gamma quanta. This usually happens in the picosecond range but can also occur several minutes or more after the initial alpha or beta decay. Rotational and vibrational energy levels of an atomic nucleus have discrete and characteristic energies. This makes it possible to draw conclusions on the isotopes contained in the measured material by measuring the emitted gamma radiation. This technique is referred to as gamma spectroscopy.

Compared to alpha or beta radiation, gamma radiation has a much higher ability to penetrate matter due to electrical neutrality of photons. The intensity of the radiation decreases exponentially with the penetration depth. The determinable half-value thickness is highly dependent on the atomic number of the respective shielding material. There are three predominant interaction mechanisms with matter:

- *Photoelectric effect*
  The photoelectric effect is an example of photo-ionization, i.e. the ionization of an atom or molecule through the absorption of electromagnetic radiation. In the case of the photoelectric effect, an inner shell electron is emitted while the incident photon is absorbed. The difference between the photon energy and the binding energy of the electron is transferred to the emitted electron as kinetic energy. The photo absorption coefficient, which describes the probability for this effect, increases with decreasing photon energy, increasing atomic number of the target material and increasing target density. If the incident photons energy is lower than the binding energy of an electron of a specific shell (e.g. K-shell electron), absorption by this electron is not possible. If the energy of the photon reaches the binding energy of an atomic shell, interaction probability increases abruptly, which leads to the formation of absorption edges (Fig. 2).

- *Compton scattering*
  With Compton scattering the incident photon transfers only a portion of its energy to an outer shell electron, which is released in this process. Compton scattering

is an example of inelastic scattering. Both the scattered photon as well as the emitted electron have to be taken into account from an radiological standpoint. The probability for Compton scattering is dependent on the photon energy as well as the target density. In an energy range between 0.2 and 10 MeV the Compton scattering coefficient can be described as follows (with n = 0.5 to 1):

$$\sigma_c \propto \rho \frac{Z}{A \cdot E_\gamma^n} \approx \rho \frac{1}{E_\gamma^n} \tag{2.4}$$

- *Pair production*

  Pair production is the transformation of a high energy photon into a electron-positron-pair, whereby the incident photon is annihilated in this process. For pair production near a nucleus, the photon energy has to be greater than the corresponding rest mass energy of two electrons. Accordingly, this process only occurs at a photon energy above 1,022 keV (Eq. 2.5).

$$E_\gamma = 2m_e c^2 = 1022\ keV \tag{2.5}$$

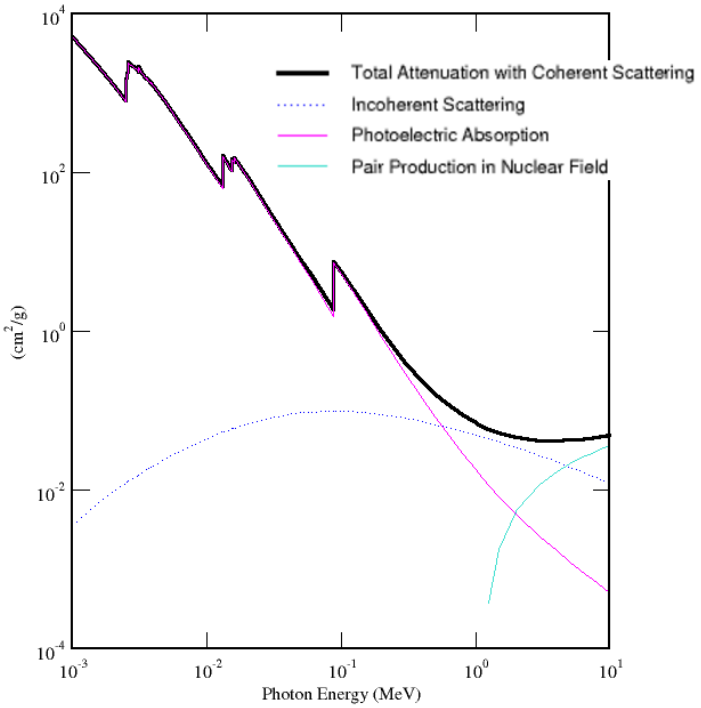

Fig. 2: Absorption coefficient lead [4]

2.1.4 Neutron radiation

Another category of ionizing radiation is neutron radiation. In order to be able to qualitatively describe the effects of neutron radiation, it is necessary to go more in depth on this topic, which is done in Chapter 2.2.

2.2 Neutron Physics

The neutron is a subatomic particle which, alongside with the proton, forms the nucleus of an atom. It is charge-neutral and has a rest mass of $1.675 * 10^{-27}$ kg, which is slightly high than that of the proton [5]. Since the neutron has a larger rest mass than proton and electron together, the decay of a neutron is energetically possible. In fact, free neutrons are unstable and decay with a half-life of about 10.2 minutes via β^--decay into a proton, an electron and an electron antineutrino. [6]

Both protons and neutrons have an internal structure, which is formed by elementary particles - quarks. However, for this paper, the internal structure of the nucleons is not of immediate importance, so it will not be discussed further here.

The main interest in reactor engineering and reactor physics generally applies to the interaction between neutrons and atomic nuclei. In order to be able to describe this interaction and the various mechanisms, the underlying concepts must be described first.

Since the neutron itself has no charge, the electrical charge of electrons in the atomic shell or protons in the atomic nucleus has no effect on it. The interaction of neutrons with matter takes place via the strong interaction, which acts upon protons and neutrons, but not on electrons. Therefore, free neutrons do not interact with the atom as a whole, but only with the atomic nucleus. The strong interaction has a range of only a few femtometers, which is why interactions between neutrons and matter occur much less frequently than with charged particles that interact via the long-range Coulomb force, or photons, which can also interact with electrons of the atom shell in addition to the atomic nucleus.

2.2.1 Neutron Energy

As described in the following chapter, the interaction probability between matter and neutron strongly depends on the neutrons energy. Due to this fact, it is obvious to define different energy ranges for neutrons. Depending on the application, these ranges can be selected to be arbitrarily fine, however, in reactor physics a distinction is generally made between three different ranges:

- *Thermal neutrons* have a kinetic energy of 0.025 eV, which corresponds to a temperature of around 293 K. The comparison between kinetic and thermal energy leads to the fact that neutrons in this energy range are in thermal equilibrium with the surrounding medium.
- Epithermal neutrons have energies that fall within the range in which resonances occur (Chapter 2.2.3). This energy range is not strictly defined and can range from meV to MeV.
- Fast neutrons have energies greater than 1 MeV. Neutrons in this energy range are the result of nuclear reactions, e.g. nuclear fission, which is why these neutrons are also referred to as fission neutrons.

2.2.2 Cross-section

In order to be able to quantitatively describe the interaction probability between neutron and atomic nucleus, the cross-section concept is introduced. However, the cross-section should not be mistaken with the geometric cross-section of the nucleus. It should be understood as the 'visible size' of the nucleus for the incident neutron, and may differ greatly from the actual geometric size. For example, the absorption cross-section of ^{135}Xe for thermal neutrons is $2.65 \cdot 10^{-18}$ cm^2, whereas the true geometric cross-section is $1.29 \cdot 10^{-24}$ cm^2 - a difference of over six orders of magnitude [7]. Since the cross-section is generally a very small quantity, the barn was chosen as standard unit. One barn corresponds to $1 \cdot 10^{-24}$ cm^2. The microscopic cross-section is denoted σ.
The neutron cross-section is generally not constant and depends on the following factors:

- The cross-section is strongly dependent on the respective target element, although there may also be a significant difference between different isotopes.

- Different reaction types, which are described in more detail in Chapter 2.2.3, also show different cross-sections.

- The cross-section has a strong dependence on the energy of the incident neutron. According to the energy classification in Chapter 2.2.1 different ranges are defined for the cross-section [8]:

  - $1/\sqrt{E}$*-region*: In the range of thermal neutron energies, the cross-section shows a $1/\sqrt{E}$-dependence. This can be explained by the fact that at lower velocities the neutron spends more time in the vicinity of the nucleus and thus the interaction probability increases towards lower energies.

  - *Resonance region*: As described in Chapter 2.1.3, atomic nuclei have discrete energy levels. If the energy of the incident neutron falls within the range of these energy levels, interaction probability increases strongly. Towards higher energies, the gaps between excitation levels of the nucleus become smaller.

  - *Fast region*: Above a certain energy, the width of individual resonances becomes greater than the gap between each other, which causes the cross-section to go back to a continuum. In general, the cross-section continues to decrease towards higher energies.

- The energy of the target nucleus plays an additional role for the cross-section. As temperature of a material increases, so does the thermal motion of the atomic nuclei. The resulting different relative velocities between nucleus and neutron lead to a broadening of the cross-section resonances, which is referred to as Doppler Broadening. As a result, resonances are effective in a broader energy range and the interaction probability between nucleus and neutron increases.

Fig. 3 shows some examples for the described dependencies of the cross-section.

2.2.3 Interaction types

There are various types for interaction between neutron and matter. In principle, a distinction is made between scattering, absorption and transfer reactions. Scattering is further differentiated between elastic and inelastic scattering. The absorption of a neutron may be followed by various processes, such as the emission of one or more gamma quanta,

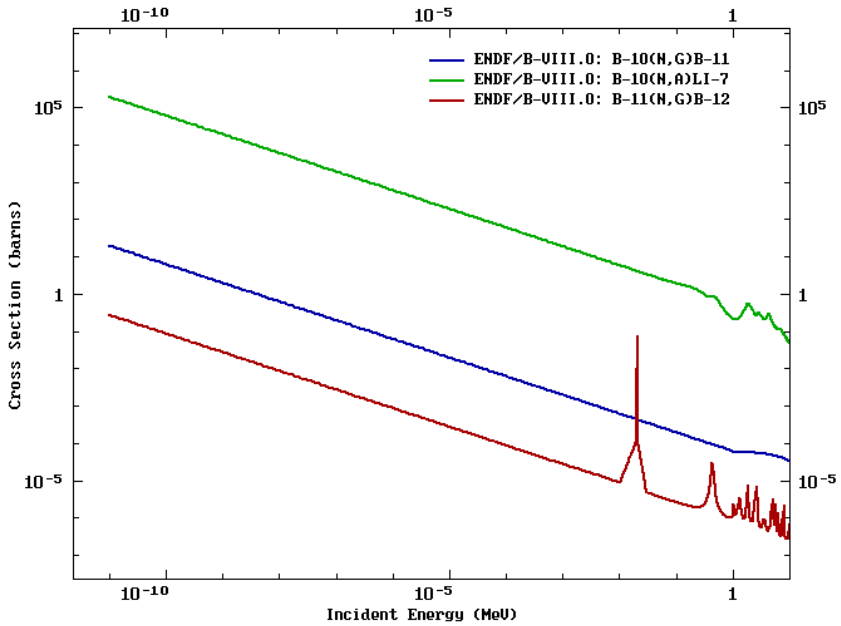

Fig. 3: Cross-section data B^{10}/B^{11} for different interaction types [6]

another particle (e.g. proton), or spontaneous fission. For each of these processes, a separate cross-section is defined, which, when combined, gives the total cross-section. In the following, the various reaction types are discussed.

Scattering

Scattering occurs, when a neutron interacts with a nucleus and a single neutron is emitted. These two neutrons may not necessarily be the same, but the net effect is as if the incident neutron were scattered by the target nucleus. There are two categories for scattering:

- Elastic scattering σ_e

  In elastic scattering processes, kinetic energy and momentum of the system is conserved. The neutron transfers some of its translation energy to the target nucleus. The target nucleus itself however remains in its ground state.

- Inelastic scattering σ_i

  As with elastic scattering, inelastic scattering leads to the transfer of translational energy. In addition, however, part of the kinetic energy of the incident neutron is converted into excitation energy of the target nucleus. This excitation energy is released after a certain time, depending on the lifetime of the excited state, in the form of one or more gamma quanta.

In both scattering processes, the target nucleus stays the same after the interaction, including possible gamma emission, is completed.

Absorption

Absorption of a neutron usually leads to the production of an unstable compound nucleus. This compound nucleus then emits a charged particle or gamma ray and leaves a daughter nucleus with different mass number, which can also be radioactive. Different absorption processes are described in the following.

- Radiative capture σ_c
  Radiative capture means the complete absorption of the incident neutron, the newly formed nucleus is in an excited state. This excitation energy is dissipated by the emission of one or more gamma quanta.

- Particle ejection
  This process results in the absorption of a neutron, followed by the emission of a charged particle, e.g. proton or α-particle, or one or more neutrons. After the particle emission, the daughter nucleus can remain in an excited state and undergo further decay.

- Fission
  For certain nuclides, neutron absorption leads to fission of the absorbing target nucleus. However, this process is not to be understood as spallation of the target. Rather, the absorption of a neutron, and the energy thus introduced into the atomic nucleus, by a fissile nuclide leads to instability and eventually to rupture of the nucleus. Since nuclear fission plays a central role for this paper, this process is explained in more detail in Chapter 2.3.

2.2.4 Attenuation

In order to be able to quantitatively describe the attenuation of a neutron beam in matter, we assume a target with thickness dx and an area A (Fig. 4). With the particle density N_X, the total number of particles in the target is

$$n_X = N_X A\, dx. \tag{2.6}$$

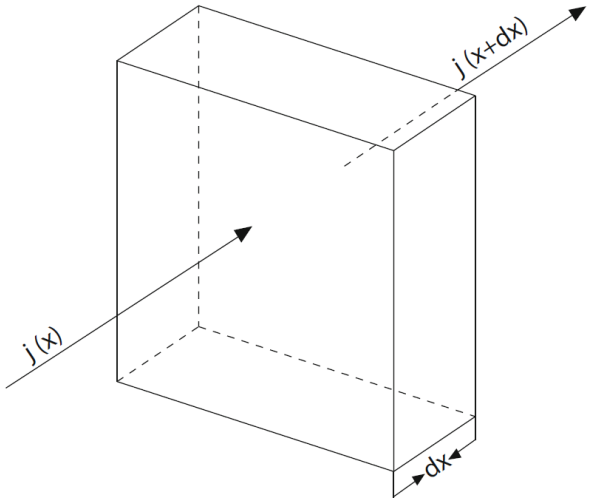

Fig. 4: Neutron beam attenuation [8]

With the definition of the cross-section σ (Chapter 2.2.2), this results in a total area visible to the neutron beam of

$$dF = N_X F \sigma \, dx. \tag{2.7}$$

Assuming that dn_a neutrons interact with the target per second, this results in the interaction probability

$$\frac{dn_a}{n_a} = N_X \sigma \, dx. \tag{2.8}$$

For the incident neutron beam $j(x)$ this means an attenuation in the layer dx of

$$\frac{dj}{j} = -N_X \sigma \, dx. \tag{2.9}$$

The solution to this differential equation leads to the exponential attenuation of a neutron beam in matter in the form of

$$j(x) = j(0) \cdot e^{-N\sigma x}. \tag{2.10}$$

2.3 Nuclear fission

In order to understand the use of energy released by fission of atomic nuclei in nuclear power plants and the associated aspects relevant to this paper, it is necessary to describe the required processes in more detail. In this chapter the physical principles of nuclear fission are explained, a description of the technical implementation can be found in Chapter 3.

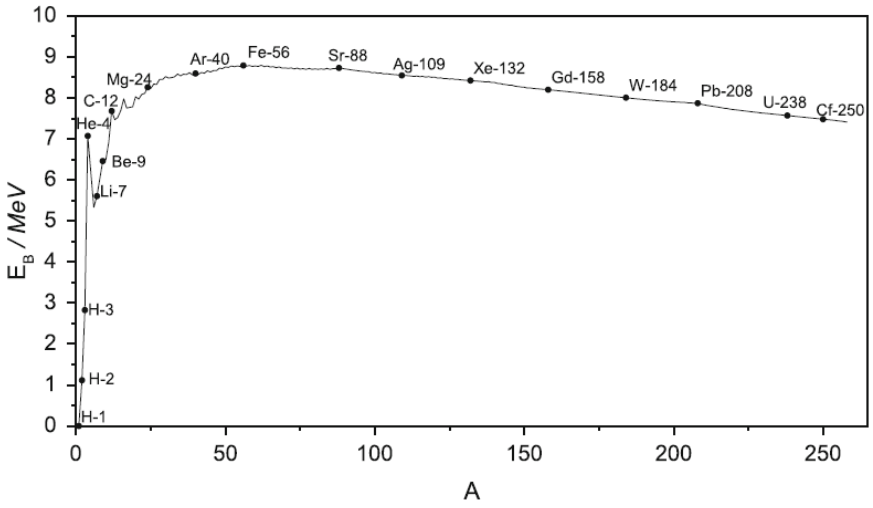

Fig. 5: Binding energy per nucleon [8]

2.3.1 Fission process

In Fig. 5, the binding energy per nucleon, which can be calculated from the mass defect (Eq. 2.11), is plotted as function of the mass number. As can be seen, the binding energy per nucleon reaches a maximum at a mass number of around 60. This means that fusion of lighter and fission of heavier nuclides leads to more stable configurations.

$$\Delta M = Z(M_p + m_e) + NM_n - (M_A + Zm_e) \tag{2.11}$$

A closer examination using the semiempirical Bethe-Weizsäcker formular (Eq. 2.12) shows that the decrease in binding energy per nucleon in heavier nuclides is due to the greater increase in Coulomb repulsion compared to the attraction through strong interaction. [9]

$$E_b = a_V A - a_S A^{2/3} - a_F (N-Z)^2 \cdot A^{-1} - a_C Z^2 \cdot A^{-1/3} + \delta \cdot a_p A^{-1/2} \tag{2.12}$$

Although fission of heavy nuclides can also happen spontaneous, i.e. without external influence, this occurs only rarely. This is because a certain activation energy, also called critical energy, is required to initiate fission of the nucleus. The necessary energy can be inserted into the nucleus via different processes, but the most important process is neutron absorption. Tab. 1 shows the critical energy as well as the binding energy of the last

Compound Nucleus	Critical Energy	Binding Energy of Last Neutron
^{234}U	4.6	6.6
^{236}U	5.3	6.4
^{239}U	5.5	4.9

Tab. 1: Critical energy and binding energy of last neutron, in MeV [10]

neutron for different isotopes of Uranium. As can be seen, for ^{236}U the critical energy is 5.3 MeV, while the binding energy of the last neutron is 6.4 MeV. This means that upon absorption of a neutron by ^{235}U, the extra binding energy of the neutron already exceeds the critical energy and no additional energy in form of kinetic energy of the neutron is necessary. For ^{238}U, however, the neutron must have a kinetic energy of at least 0.6 MeV to achieve fission of the compound nucleus ^{239}U. Since fission of ^{235}U is of major importance in light-water reactors, the fission process for this nuclide is further explained below.

As described above, the absorption of a thermal neutron leads to the formation of the excited compound nucleus ^{236}U. The excitation energy causes the newly formed nucleus to oscillate. If the energy introduced by the neutron is large enough, as is the case for ^{236}U, the oscillation will cause the nucleus to become dumbbell-shaped. Above a certain distance between the two segments, the repulsive Coulomb interaction exceeds the attractive strong interaction at the constriction, which leads to fission of the nucleus. In Fig. 6, different deformation forms are shown. The two fragments are driven apart after fission by the Coulomb force and are also in highly excited states. This excitation energy is dissipated by emission of neutrons and γ-rays.

2.3.2 Fission products

The mass distribution between the two fission products is generally asymmetric. The independent fission yield describes the yield for fission products directly after the fission process, while the cumulative fission yield considers decay of preceding nuclides (see Fig. 7). The fission products usually have a strong neutron surplus, which is dissipated through successive β^--decays, and are therefore also radioactive.

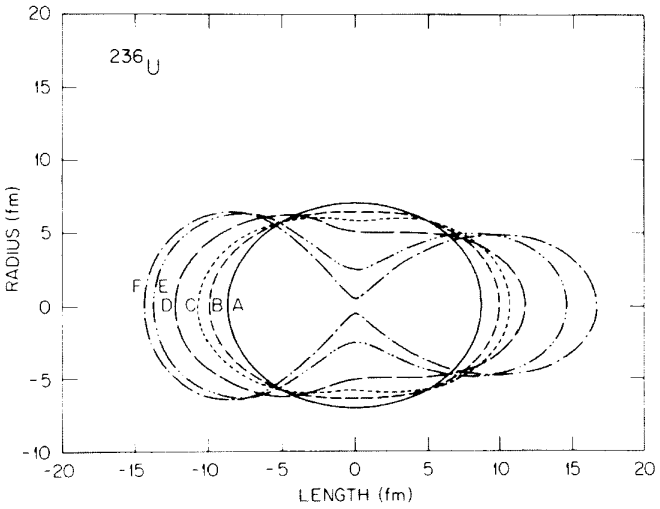

Fig. 6: Deformation of ^{236}U [11]

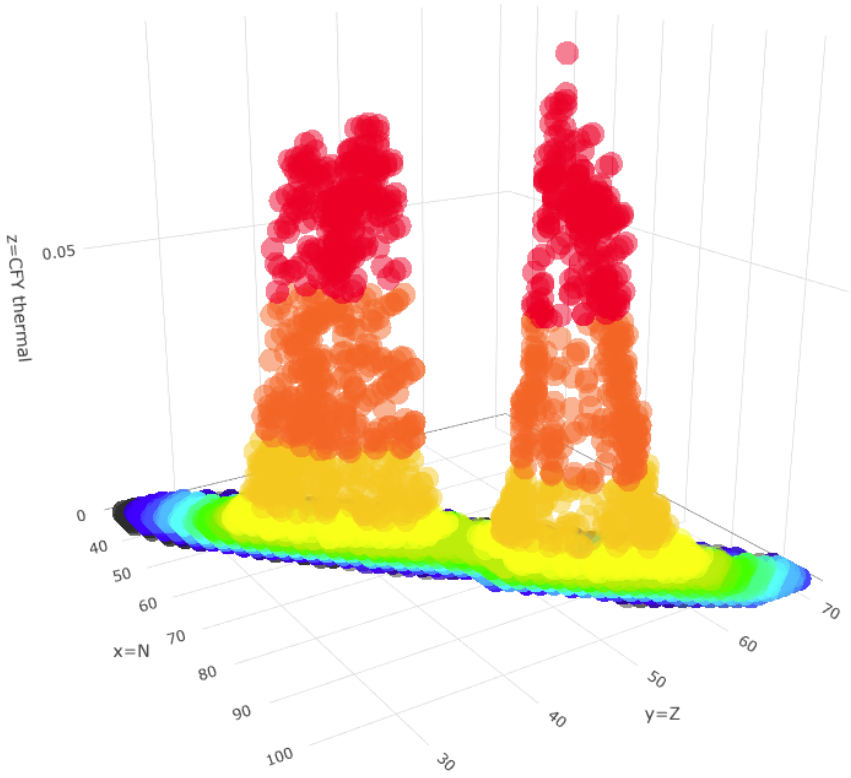

Fig. 7: Cumulative fission yield for thermal fission of ^{235}U [12]

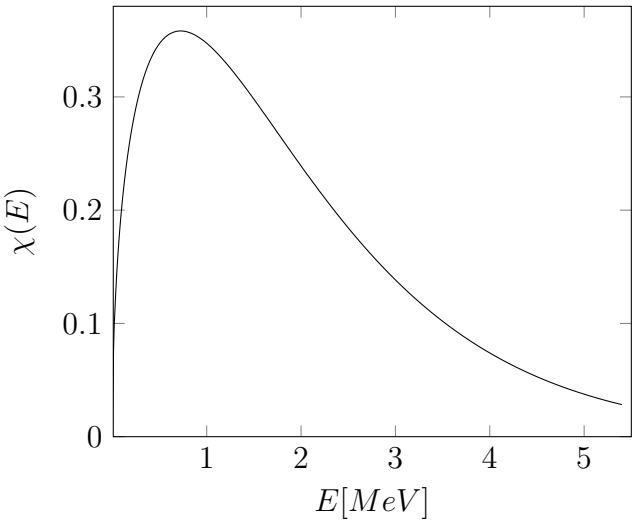

Fig. 8: Fission neutron energy spectrum for fission of ^{235}U [10]

2.3.3 Neutron Production

In addition to fission products, neutrons are also emitted during the fission process of the compound nucleus. These neutrons are necessary to maintain the chain reaction in the nuclear reactor. More than 99% of the generated neutrons are emitted more or less instantaneously during the fission process and are called prompt neutrons. The time between fission-inducing neutron absorption and emission of the prompt neutrons is about 10^{-14}s, which corresponds to the lifetime of the formed compound nucleus ^{236}U. The energy spectrum of prompt neutrons can be determined using Eq. 2.13 and is plotted in Fig. 8. On average, 2.43 prompt neutrons are generated per fission, with a mean energy of 1.98 MeV [10].

$$\chi(E) = 0.453e^{-1.036E}sinh\sqrt{2.29E} \tag{2.13}$$

However, a small proportion of the total neutrons produced is emitted with some delay and are called delayed neutrons. This is because these neutrons are released by fission products that do not occur directly through the fission process but are formed by preceding β^--decay. The time interval between fission and emission of delayed neutrons depends on the half-life of the preceding nuclides and can be between a few milliseconds to up to minutes. The delayed neutrons are divided into six groups depending on the half-life (Tab. 2). Although delayed neutrons only contribute a small fraction to the total neutron balance, about 0.64%, they play an important role in the control of the chain reaction.

Group	half-life (s)	neutrons per fission
1	55.72	0.00052
2	22.72	0.00346
3	6.22	0.00310
4	2.30	0.00624
5	0.61	0.00182
6	0.23	0.00066

Tab. 2: Delayed neutrons with thermal fission of ^{235}U

The delayed neutrons extend the reactor period, i.e. the time in which the total neutron number increases by a factor e, from 0.2s to about 20s. [13] In addition, in a nuclear reactor, other neutron producing reactions occur, such as (γ,n)- and (n,2n)-processes, which also contribute to the neutron balance.

2.3.4 Moderation

The fission cross-section and the total neutron cross-section of ^{235}U are shown in Fig. 9. As can be seen, the fission cross-section behaves as described in Chapter 2.2.2. As described above, the prompt neutrons have an energy of about 2 MeV. It is obvious, that in this energy range parasitic absorption predominates, which would prevent a self-sustaining chain reaction. Therefore, to enable continuous operation of a reactor using ^{235}U as its fuel, it is necessary to decelerate the generated neutrons into the thermal energy range. This process is called moderation. In light water reactors, which include the pressurized water reactor relevant to this thesis, this deceleration is accomplished by water via elastic collisions between neutrons and mainly hydrogen atoms. For hydrogen, an average of 18 collisions is required per neutron to moderate it from 2 MeV to 25 meV. Furthermore, it is necessary to keep the parasitic absorptions in the moderator itself as low as possible, i.e. the ratio between elastic scattering and total cross-section should be close to 1. As can be seen in Fig. 10, this is the case both for hydrogen and oxygen. In other reactor types, moderation is realized by different materials, such as graphite.

2.3.5 Criticality

In general, for continuous operation of a nuclear reactor, it is necessary that the number of neutrons per unit volume and time remains constant. This circumstance is described

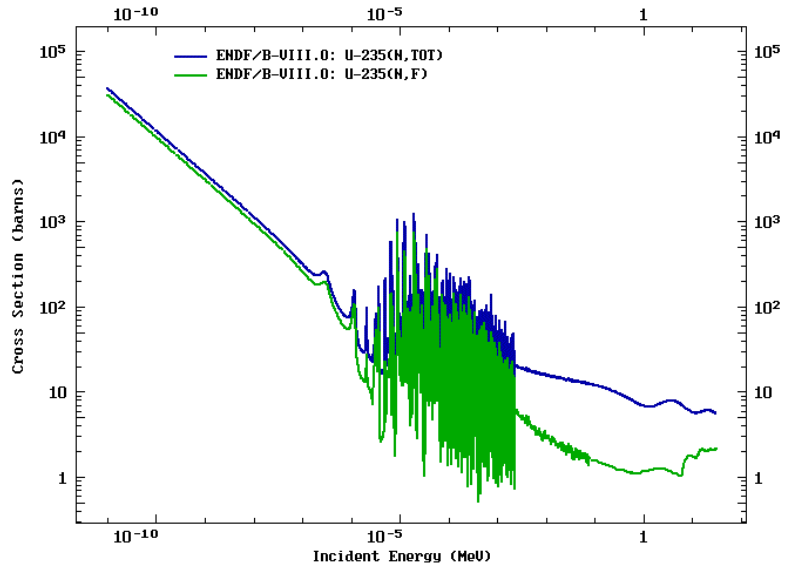

Fig. 9: Fission cross-section and total cross-section of ^{235}U [6]

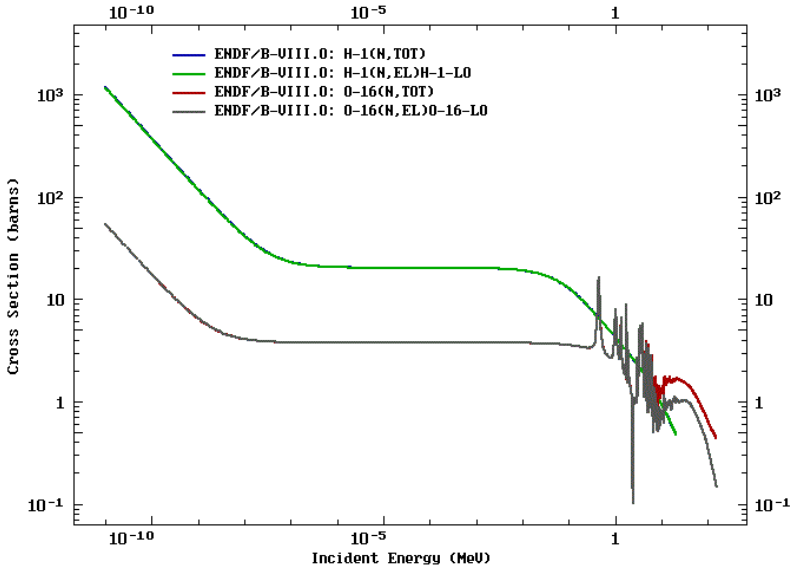

Fig. 10: Elastic scattering and total cross-section for ^{1}H and ^{16}O [6]

^{233}U	^{235}U	^{239}Pu	^{241}Pu
2.49	2.42	2.87	2.93

Tab. 3: Values for η for thermal fission [13]

by the multiplication factor k.

$$k = \frac{\text{neutron population of generation i}}{\text{neutron population of generation i-1}} \tag{2.14}$$

In order to achieve a chain reaction, k must be greater or equal to 1. For $k < 1$, the number of neutrons in the considered volume decreases after each neutron generation. The main influences on this factor are described in the following:

- The thermal utilization f describes the ratio between absorbed neutrons in the nuclear fuel and the total number of neutrons absorbed, i.e. in the nuclear fuel and other materials.

$$f = \frac{\text{absorption of thermal neutrons in the fuel isotope}}{\text{total number of thermal neutrons absorbed}} \tag{2.15}$$

- The reproduction factor η is the number of fission neutrons emitted per neutron absorbed in the nuclear fuel. Typical values for different fuel isotopes are listed in Tab. 3.

- Although energy generation in a light water reactor relies mainly on thermal neutron fission, some of the fast neutrons produced in the fission process lead to fission as well, mainly in ^{238}U. This circumstance contributes positively to the neutron balance and is described by the fast fission factor ϵ.

$$\epsilon = \frac{\text{number of fission processes caused by fast and thermal neutrons}}{\text{number of fission processes caused by thermal neutrons}} \tag{2.16}$$

- During the deceleration of the fission neutrons from the fast into the thermal energy range, there is a certain probability of parasitic absorption during this process. Fig. 11 shows the total neutron cross-section for ^{238}U. As can bee seen, the neutron cross-section in the resonance energy range increases strongly, consequently increasing the interaction probability. The probability that a neutron will not be absorbed during moderation is therefore described as resonance escape probability p.

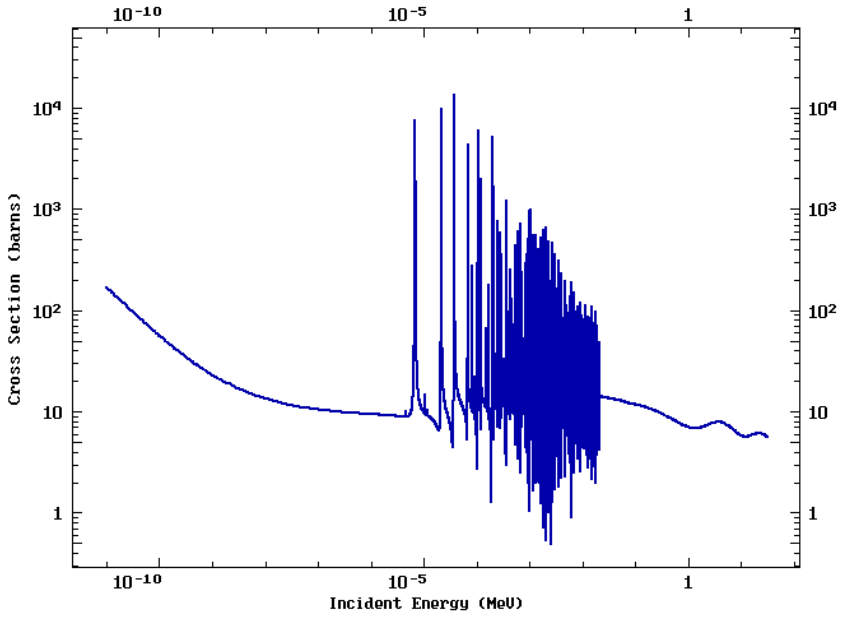

Fig. 11: Total cross-section of ^{238}U [6]

Together these factors form the four-factor formula:

$$k_\infty = f \cdot \eta \cdot \epsilon \cdot p \tag{2.17}$$

However, this formula is valid only for an infinitely extended reactor, since there is no directed neutron current, thus neutron leakage from the reactor core does not have to be taken into account. For finite expansion, this formula must be extended by the so-called non-leakage probability for fast (P_f) and thermal (P_{th}) neutrons.

The value range for k is divided as follows:

- $k < 1$ means that the number of neutrons decreases with each generation, the chain reaction is called *subcritical*.
- For $k = 1$ the number of neutrons from one generation to the next remains the same. This condition is called *critical*.
- $k > 1$ means an exponential increase in the number of neutrons between each generation. In this state, the chain reaction is described as being *supercritical*.

In general, with naturally occurring uranium, it is not possible to achieve a multiplication

factor of $k \geq 1$. An exception to this is the CANDU reactor, which is powered with natural uranium. In order to achieve a self-sustaining chain reaction in conventional light water reactors, it is necessary to increase the amount of fissile ^{235}U compared to ^{238}U. This process is called enrichment. In modern LWRs, the degree of enrichment is between 2 and 5%.

3. Reactor Design

While Chapter 2 describes basic reactor physics for this thesis, it is necessary to take a closer look at the technical fundamentals of energy and power production in nuclear power plants.

There are many different reactor concepts, which differ in the main categories fuel, coolant and moderator. The type of nuclear fuel used also determines the neutron spectrum in which the reactor operates. As can be seen in Fig. 12, the majority, more than 80%, of nuclear power plants in operation are designed as light water reactors (LWR). This concept uses fuel in form of enriched ceramic uranium dioxide (UO_2) and normal water both as coolant and for neutron moderation. This reactor concept operates in thermal neutron spectrum.

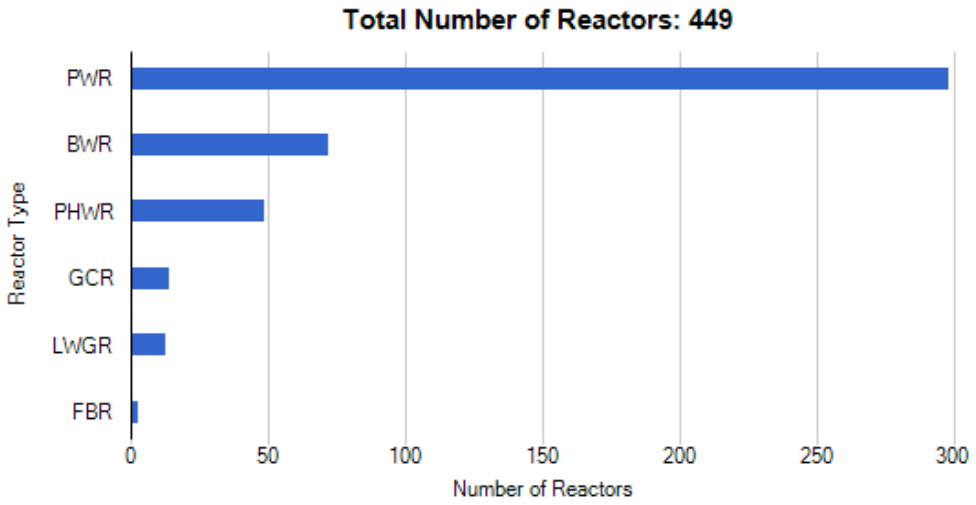

Fig. 12: Operational nuclear reactors world wide [14]

The two design options as boiling water reactor (BWR) and pressurized water reactor (PWR) differ in that in the BWR steam production for driving the turbine takes place directly in the primary circuit. In the PWR design, however, the water in the primary circuit is kept under higher pressure, which prevents boiling. Instead, the heat of the primary circuit is passed through steam generators to a secondary circuit in which steam is generated, which eventually drives the turbine. Schematic representations of these two LWR concepts are shown in Fig. 13 and 14.

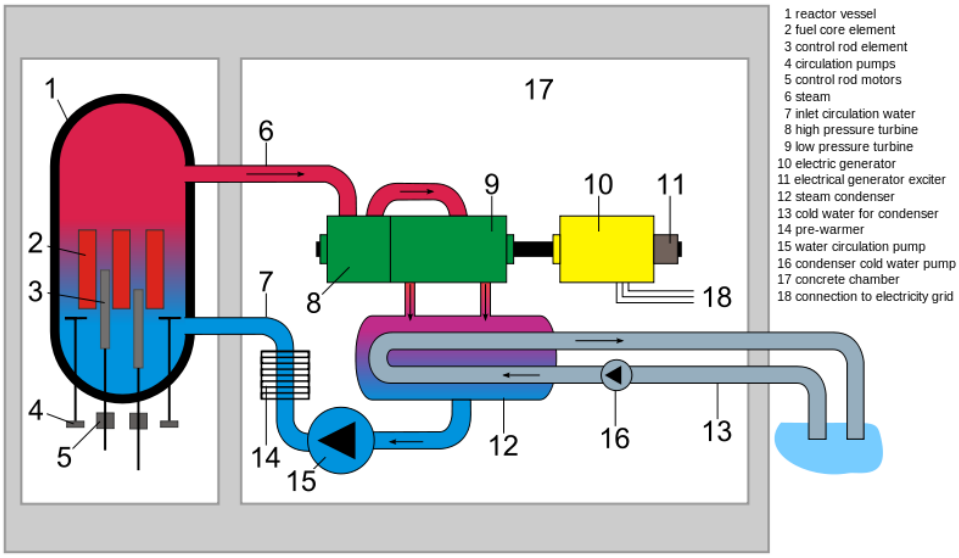

Fig. 13: BWR concept [15]

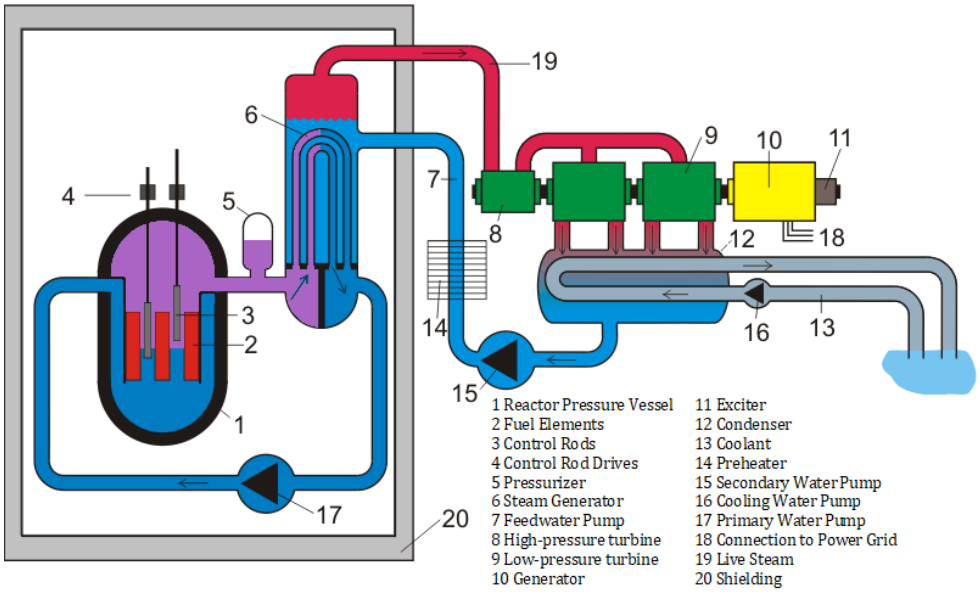

Fig. 14: PWR concept [16]

Subsequently, this thesis focuses on the pressurized water reactor. The description of this reactor concept is limited to the primary circuit, components of the secondary circuit will not be discussed. In addition to the description of the reactor and fuel assemblies in more details, a brief overview over other primary circuit components will be given.

3.1 Fuel

3.1.1 Fuel Elements

The fuel elements play a central role in the operation of a nuclear power plant. On the one hand, they must enable a self-sustaining chain reaction, which effects both the choice of materials used and the actual geometric arrangement. At the same time, the fuel assemblies must meet the safety requirements under the given operational conditions. In addition, economic requirements are placed on the fuel assemblies to ensure efficient usage.

The fuel element of an AP1000 PWR, which is referenced in the following and for which the calculations described in Chapter 5 have been carried out, are designed in a 17×17 matrix form. Here, 264 of the 289 positions are filled with fuel rods, which are discussed in Section 3.1.2. Of the remaining positions, 24 are reserved as guide tubes for insertion of control rod assemblies or burnable absorbers and the central position for instrumentation positioning. Fig. 15 shows the arrangement of such a fuel element. During operation,

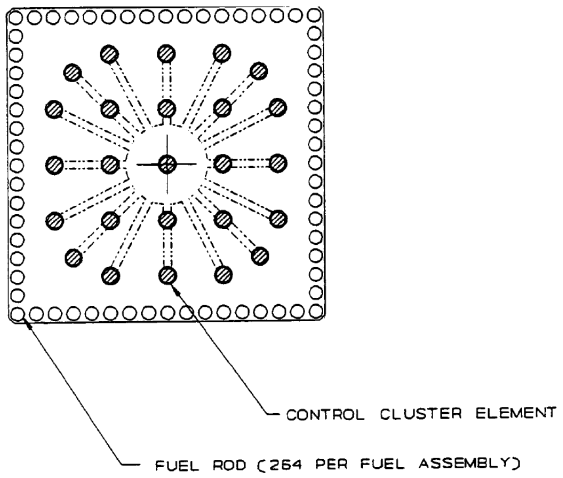

Fig. 15: AP1000 fuel assembly cross-section [17]

the coolant flows from bottom to top in the spaces between the fuel rods and guide tubes and thus ensures the transport of heat generated during the fission process and necessary moderation of fission neutrons at the same time. To ensure stability of the fuel assembly and optimal distribution of the coolant, each fuel element is equipped with fourteen spacers, including top and bottom nozzle (Fig. 16).

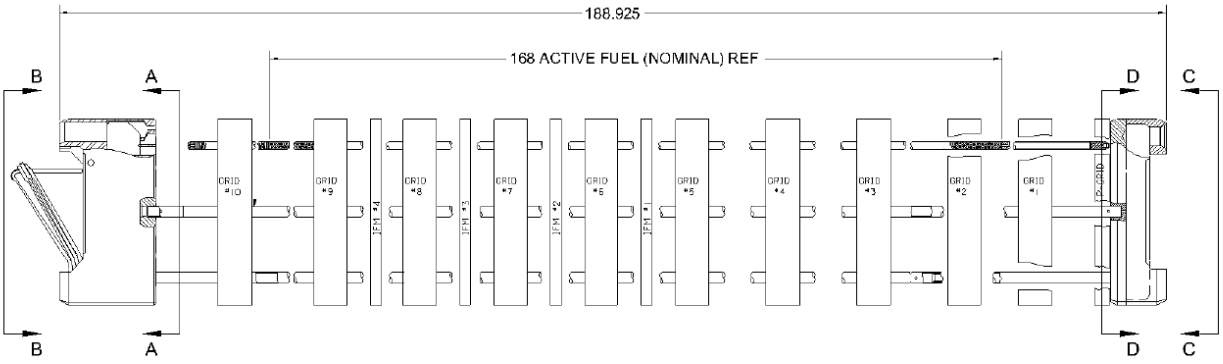

Fig. 16: AP 1000 fuel assembly, dimensions in inches [17]

3.1.2 Fuel Rods

The individual fuel rods essentially consist of two components, the fuel pellet and the cladding tube.

The fuel pellet is made of sintered uranium dioxide (UO_2), with an enrichment between 2.35 and 4.45 wt% [18]. The pellets are cylindrically shaped with the ends of the pellets being concavely shaped. This allows for thermal expansion in the axial direction and also increases the volume in which gaseous fission products, which exit the pellet, can accumulate. The expansion of the pellet in radial direction is of secondary importance because of the likewise increasing diameter of the surrounding cladding tube. The melting temperature of UO_2 is 2800 K, this temperature is not exceeded during normal operation conditions. Fig. 17 shows the radial temperature distribution over the fuel rod.

For the cladding tube, which surrounds the pellet, several requirements are made. It represents an important barrier between fuel and coolant, as it prevents the transfer of fission products into the coolant and at the same time prevents the interaction between fuel and coolant. Therefore, cladding-coolant and cladding-fuel interactions must not adversely affect the integrity of the cladding tube, it must remain tight over its entire lifetime. Additionally, the cladding tube forms the thermal bridge between pellet and coolant, mechanical deformations during operation must therefore be prevented. Furthermore, the cladding must have good neutron properties in order to minimize the effect on the neutron balance in the reactor. It is therefore necessary to use a material with a low neutron cross-section. Zircaloy meets these requirements and is used in all common light water reactors.

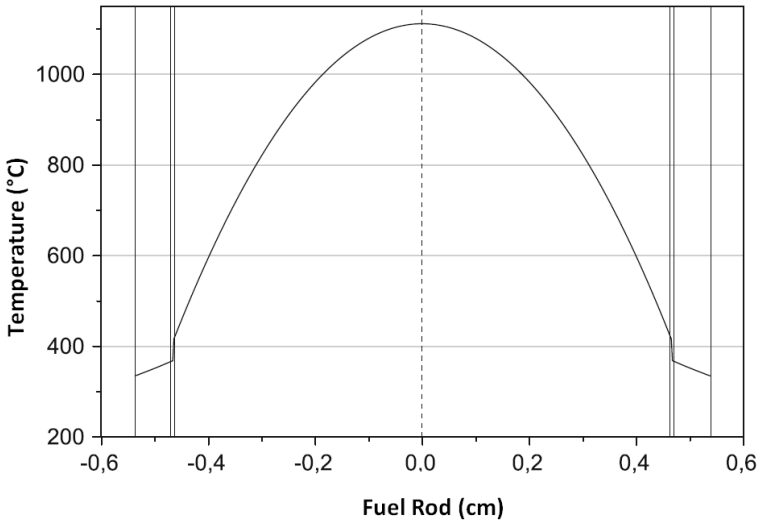

Fig. 17: Fuel Rod Temperature Distribution [8]

It is an alloy with high zirconium content, in combination with other metals such as iron, chromium and nickel [19]. In order to counteract the high coolant pressure of about 150-160 bar and therefore prevent mechanical deformation, the space between fuel pellet and cladding tube is filled with helium, which is chemically inert and has good heat transfer properties. The filling pressure at operating temperatures is 40-60 bar [8]. The active length of the fuel rods occupied by pellets, is around 4.25 m. The structure of such a fuel rod is shown in Fig. 18.

3.1.3 Control Rod Assemblies

In order to be able to control the chain reaction in the reactor core, control rods are needed. These generally consist of strongly neutron-absorbing materials such as boron or cadmium. Control rods in a PWR are used to compensate reactivity changes in the reactor during operation. These changes are generally due to burnup of the fuel rods, that is, the reduction of ^{235}U content in the fuel due to fission. Furthermore, the control rods are used for reactor shut down.

Such a control rod used in the AP1000 is shown in Fig. 19. The neutron-absorbing part of the rod consists of a silver-indium-cadmium alloy and is 4.20 m long. The cross-sections for radiative capture are shown in Fig. 20.

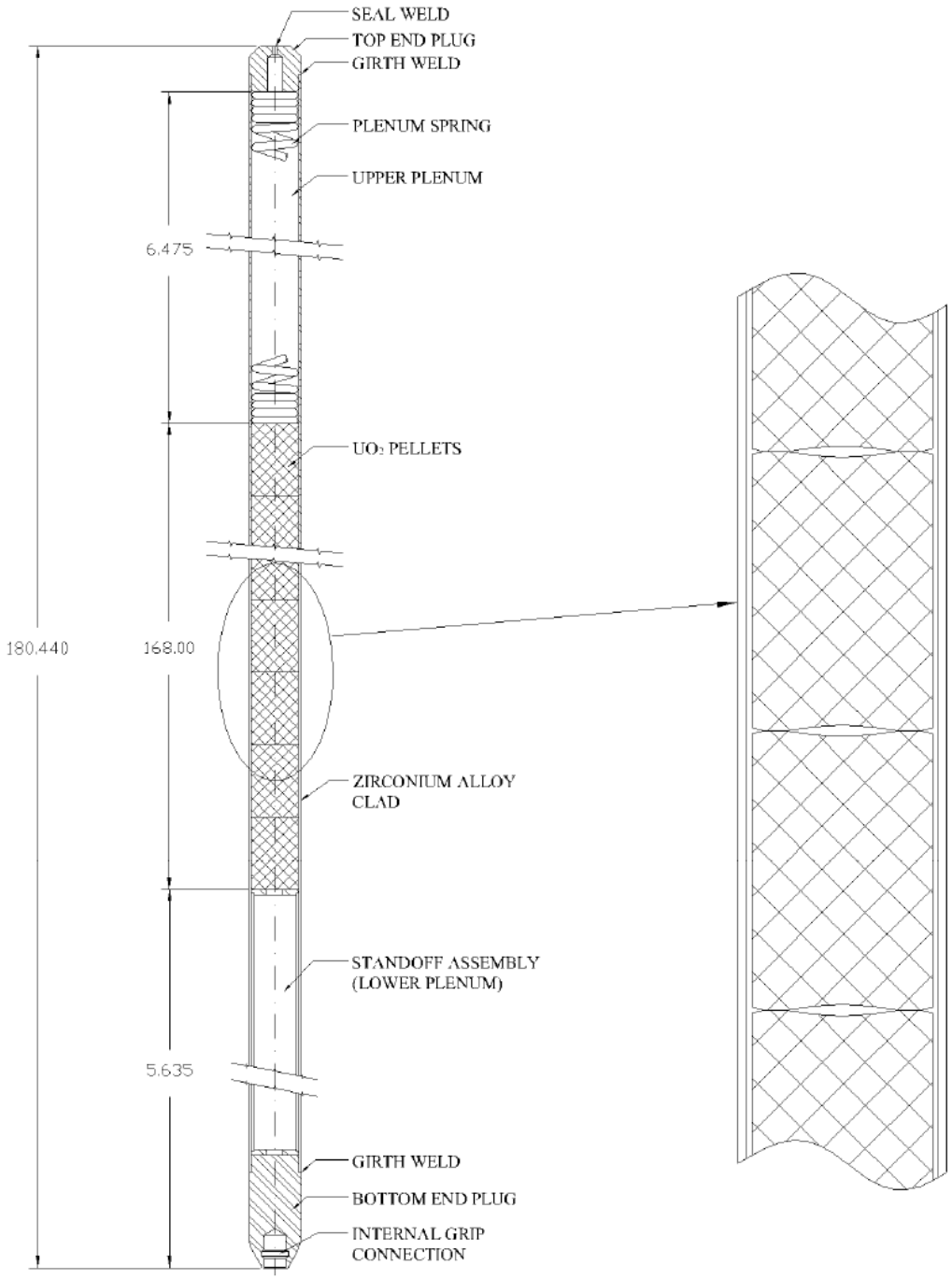

Fig. 18: AP1000 Fuel Rod, dimensions in inches [17]

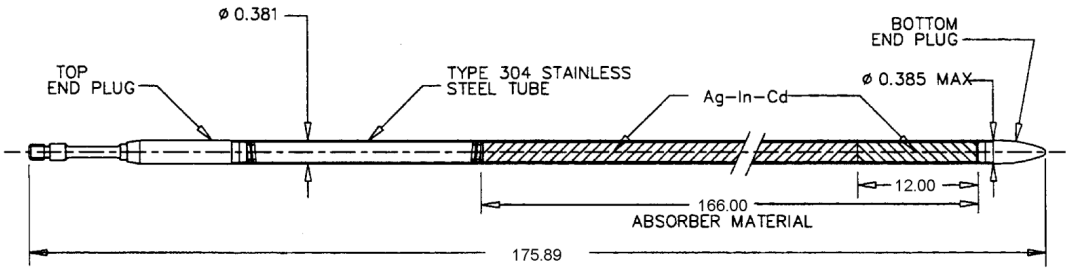

Fig. 19: AP1000 Absorber Rod, dimensions in inches [17]

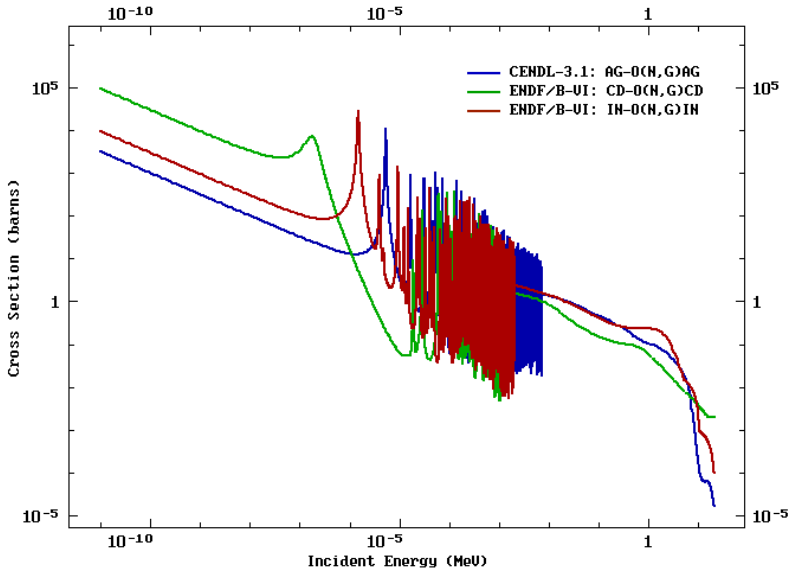

Fig. 20: Cross-sections for Silver, Indium and Cadmium [6]

The control rods are grouped into assemblies which consist of 24 individual rods in the AP1000. These control rod assemblies are inserted into the core from top directly into the guide tubes provided in the fuel assemblies. The AP1000 differentiates between rod cluster control assemblies and gray rod cluster assemblies. In the latter, only 12 of the 24 rods are designed as control rods, the rest is made of stainless steel. The two assemblies are shown in Fig 21. In total, the AP1000 uses 53 rod cluster control assemblies and 16 gray rod cluster assemblies. These assemblies are grouped into so-called "banks", which are always moved together. Fig. 22 shows the distribution of these banks in the reactor core. [18]

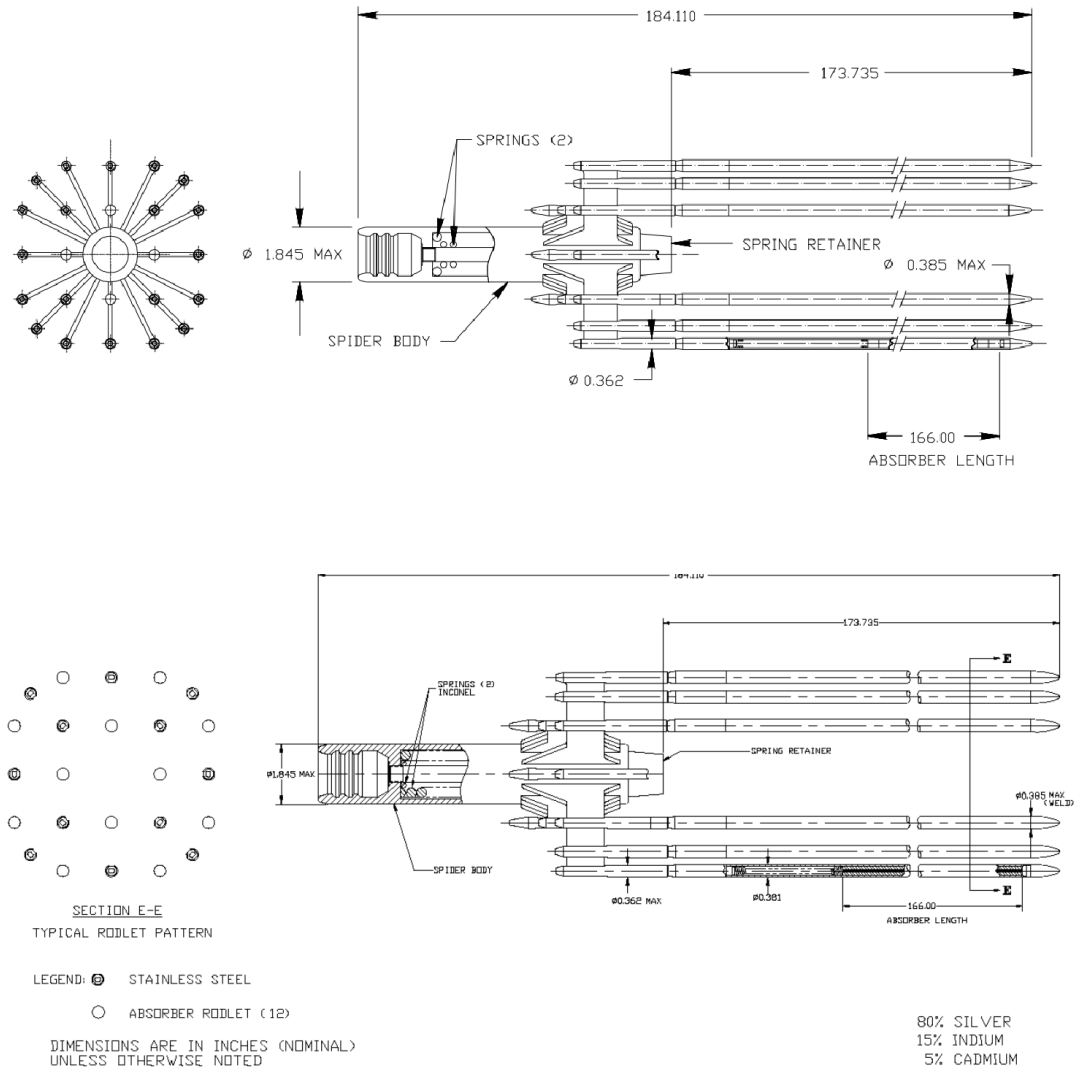

Fig. 21: AP1000 Rod Cluster Control Assemblies [17]

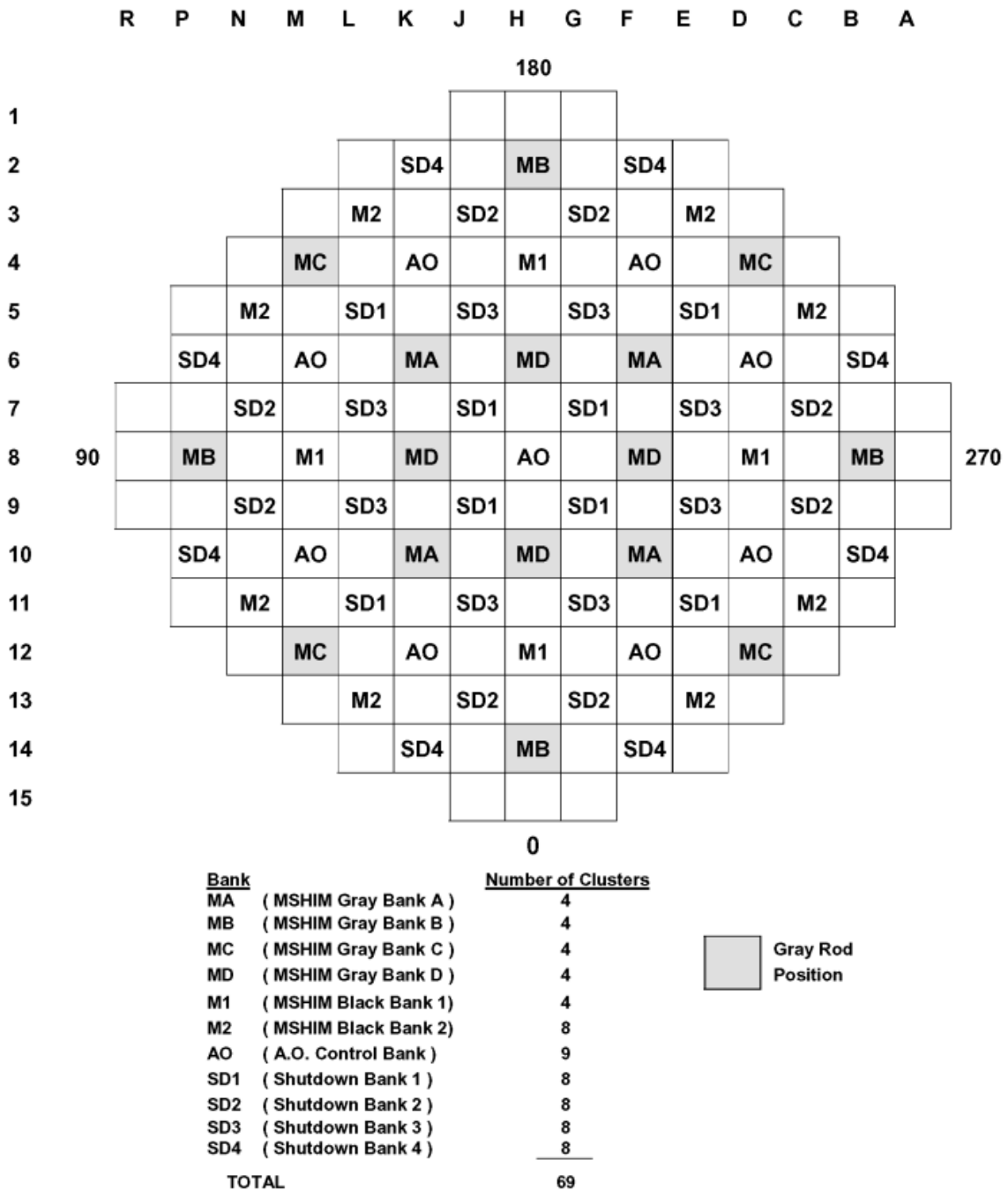

Fig. 22: AP1000 Rod Cluster Control Assembly Pattern [18]

3.2 Reactor

The components described above together with the reactor pressure vessel and its installations form the reactor. In a pressurized water reactor, the reactor forms the primary circuit together with the steam generators, the main coolant pumps and the pressurizer. In the following the pressure vessel and its internals will be discussed.

3.2.1 Reactor Pressure Vessel

The reactor pressure vessels (RPV) main task is to encase the reactor core and coolant, thereby providing one of the most important barriers to the release of radioactive material to the environment while ensuring core cooling. Furthermore, the weight of the core and various internals is transferred to the reactor pit via the RPV. In addition, the RPV plays an important role in directing the cooling flow.

Structure

The pressure vessel consists of a cylindrical center section and hemispherical heads at both ends. While the bottom head of the RPV is welded to the shell during construction, the upper part is removable, which is necessary for refueling. In addition, feed-throughs for the control rod drive mechanisms and necessary in-core instrumentation are located at the top head. In order to allow for in- and outlet of cooling water from or to the steam generators, the RPV also has in- and outlet nozzles at the upper part of the cylindrical shell. The number of these nozzles depends on the number of loops. For the AP1000 in its 2-loop version, the RPV has two inlets and one outlet nozzle per steam generator. A cross-section of the RPV at the level of those nozzles is shown in Fig. 23. At the level of the reactor core, the RPV of the AP1000 has an inside diameter of 4.04 m and a RPV wall thickness of about 22 cm. The height of the cylindrical shell is 8 m, the entire RPV has a height of 12.20 m. The total weight is 417 tons . [20] Fig. 24 shows the entire RPV.

Materials

Due to the conditions which the RPV is exposed to during operation, the highest quality requirements are placed on it. On the one hand, the mechanical stresses on the pressure vessel must be taken into account when choosing the materials used. The RPV must be able to withstand a coolant pressure of up to 170 bar and coolant temperatures of up

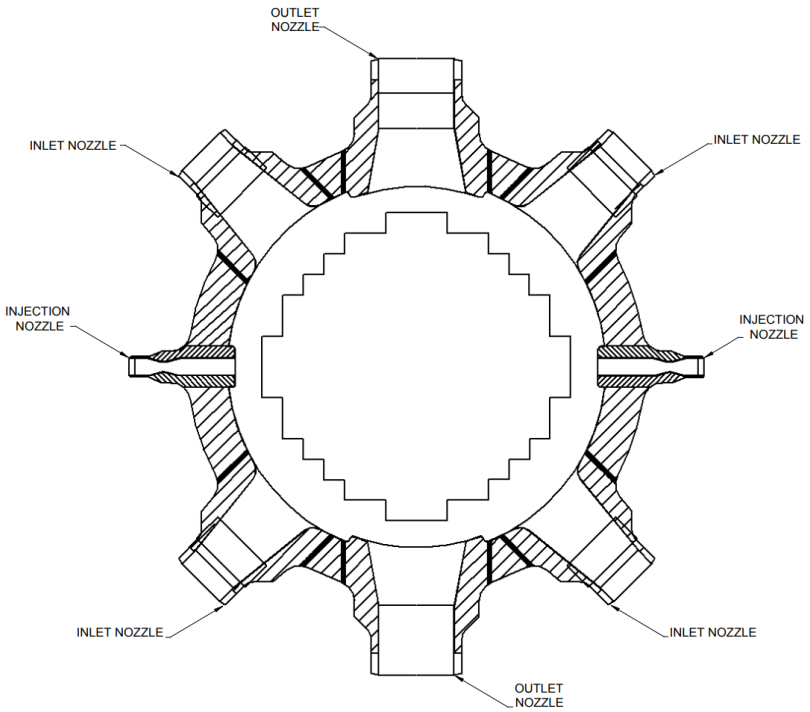

Fig. 23: AP1000 RPV Cross-Section [20]

to 350 °C. On the other hand, the radiation from the reactor core in form of neutron radiation is an important aspect as well. In addition to the activation of various isotopes of the RPV steel by radiative capture, these neutrons cause embrittlement of the material. Therefore, the content of elements such as copper, nickel and sulfur in RPV steel must be limited. A common steel for the RPV is 20MnMoNi4-5 (ASTM A553 Low Alloy Steel, Grade B, Class 1). To prevent corrosion due to contact with coolant, the RPV is provided with an austenitic stainless steel cladding about 5 mm thick.

3.2.2 RPV Internals

The internals in the reactor pressure vessel fulfill different tasks. On the one hand, the weight of the reactor core is transferred to the pressure vessel via them. On the other hand, it is necessary to direct the cooling water, which flows via the inlet nozzles into the pressure vessel, specifically to the fuel elements to ensure adequate cooling. In addition, the internals serve the protection of the RPV against excessive thermal stresses due to heat generated in the core and also against radiation damage by attenuating the neutron flux emanating from the reactor core. Fig. 25 shows the two main components.

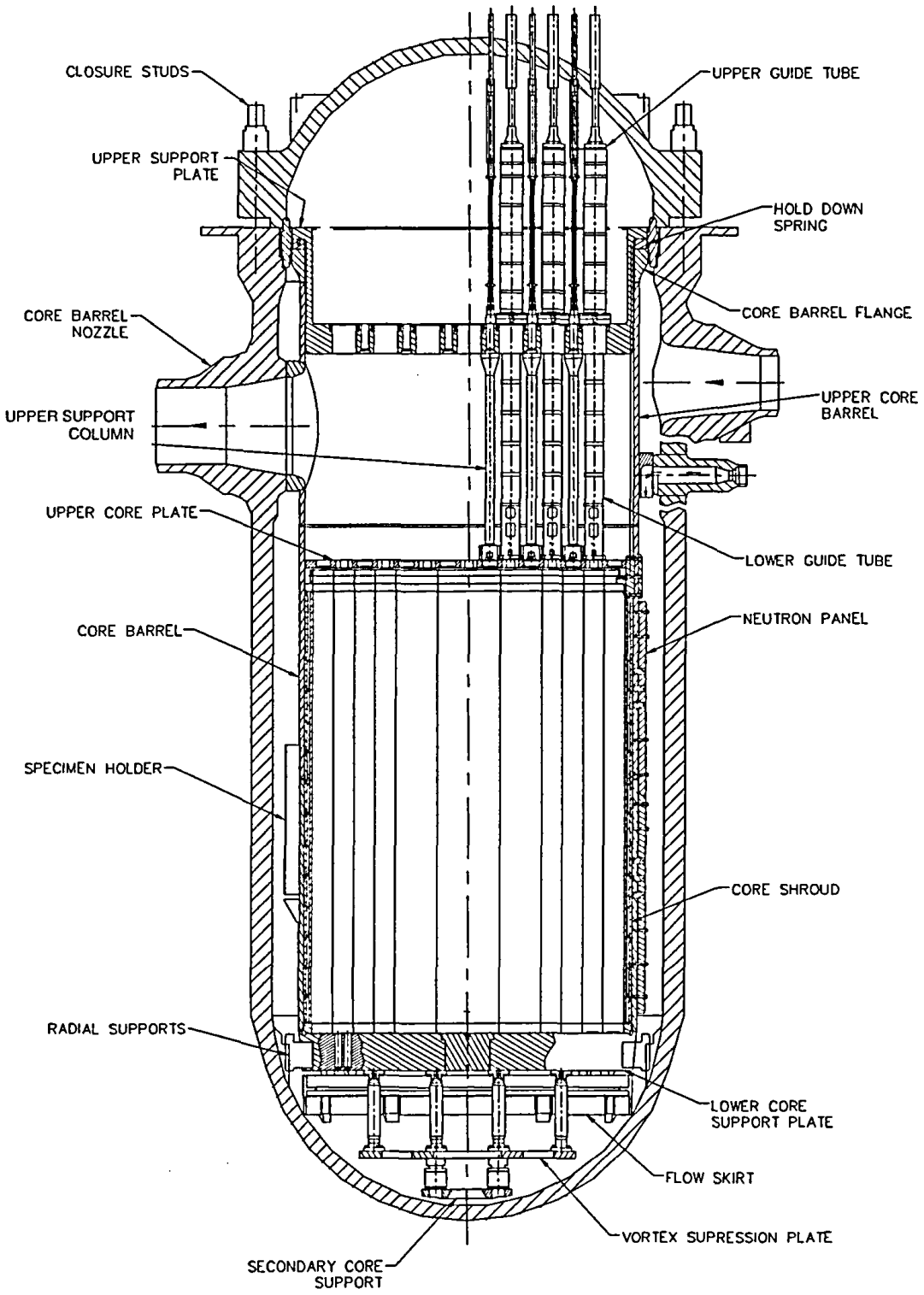

Fig. 24: AP1000 RPV [20]

Core Shroud/Baffle

The core shroud or core baffle are stainless steel plates mounted vertically on the reactor core. The core shroud retains the core support structure, in which the individual fuel elements are mounted, against lateral movements. Furthermore, the core shroud controls the flow of coolant through the reactor core. As can be seen in Fig. 22, the reactor core does not have a round shape due to the shape of the individual fuel elements. In order to keep the flow rate between the core and the core barrel as low as possible, horizontal plates, so-called formers, at regular intervals. These formers force the coolant, which enters the core from below, into the fuel element area, thus ensuring optimal flow through the core. In addition, the core shroud acts as a neutron reflector, which reduces the embrittlement of the pressure vessel. The core shroud is attached to the inside of the core barrel and is made of austenitic stainless steel.

Core Barrel

The core barrel consists of a cylindrical shell and the lower support plate, on which rests the core structure. Via the core barrel, the weight of the entire core is suspended in the pressure vessel via the radial supports and the core barrel flanges. In addition to fixating the core in the RPV, the core barrel also has the task of guiding the coolant flow. As can be seen in Fig. 24, the cooling water coming from the main coolant pumps enters the pressure vessel via the inlet nozzles and is directed downwards by the core barrel towards the RPV bottom head. Then it flows through the lower support plate into the reactor core. At the top of the core, the cooling water enters the upper core barrel area, from where it exits the RPV towards the steam generators via openings in the core barrel, which are connected to the outlet nozzles. In addition, the core barrel together with the water-filled areas between barrel and RPV as well as between barrel and shroud serves the neutron shielding of the RPV. It is also made of austenitic stainless steel.

3.3 Additional Primary Circuit Components

In the following, the other main components of the primary circuit of the AP1000 are briefly mentioned. Fig. 26 shows the entire primary circuit.

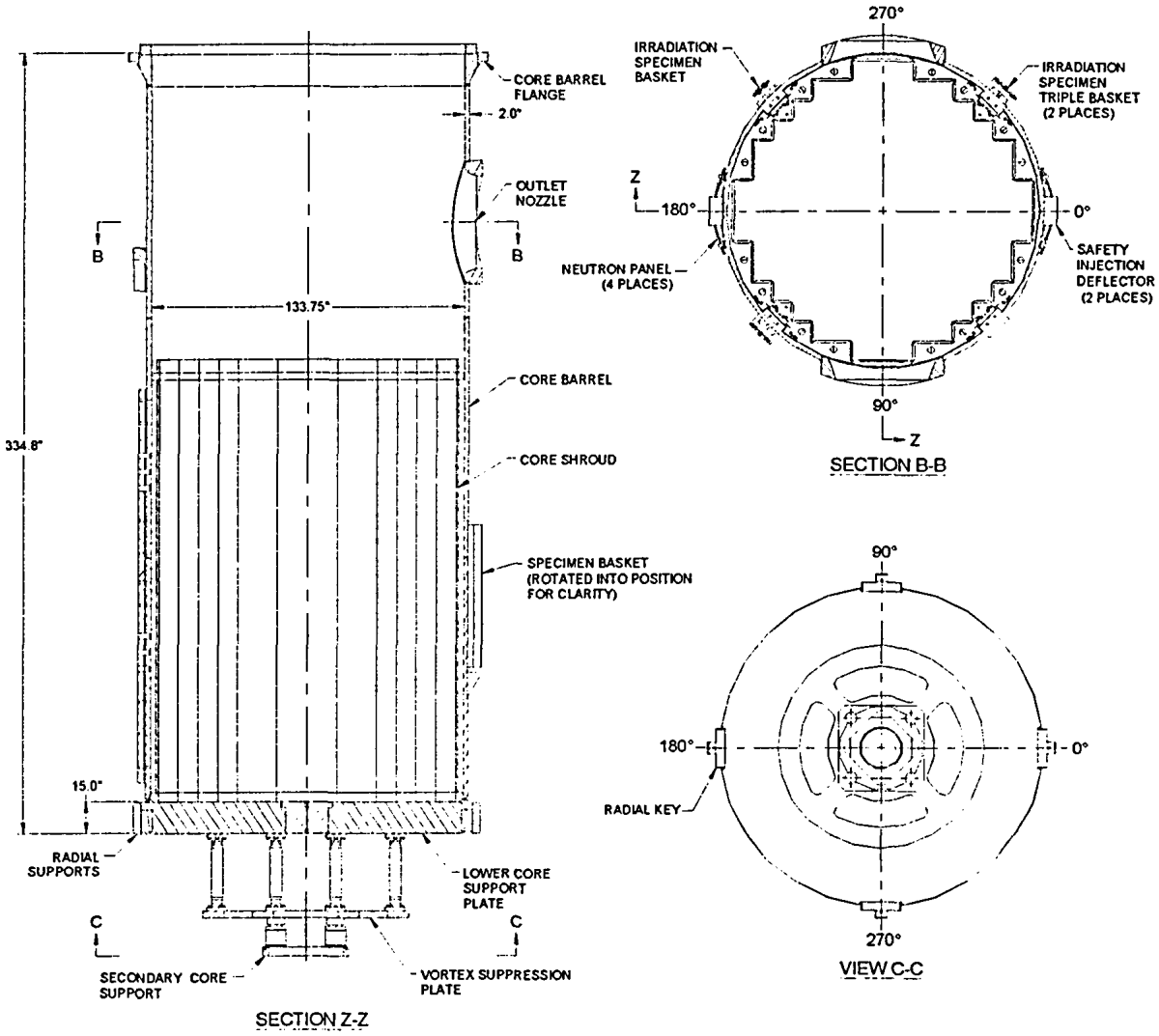

Fig. 25: AP1000 Core Barrel and Core Shroud [21]

3.3.1 Steam Generator

In the steam generators, the heat absorbed by the coolant in the reactor core is transferred to the secondary circuit. The water on the secondary side is allowed to boil inside the steam generators. The steam is dried via water separators and then directed to the turbine. The AP1000 in its 2-loop version has two steam generators, which are designed as vertical-shell U-tube evaporators and each have two cold and one hot leg. [22].

3.3.2 Pressurizer

The task of the pressurizer is to keep the pressure in the primary circuit sufficiently high and to compensate for volume changes of the coolant due to load changes during operation. For this purpose, the vertical installed pressurizer is about 50% filled with water, control over the primary circuit pressure is achieved through regulating the amount of steam above the water level. With increasing pressure, the amount of steam and thus the pressure is reduced by means of colder water, which is sprayed into the pressurizer from above. If the pressure is too low, water in the pressurizer is evaporated by means of heating elements, the amount of steam and, subsequently, the pressure in the primary circuit increase. The pressurizer is connected to the main circuit via the coolant line from the RPV to one of the steam generators. [8]

3.3.3 Main Coolant Pump

The main coolant pumps ensure adequate water supply from the steam generators to the reactor. The AP1000 has a total of four main coolant pumps installed, two per steam generator, each having a throughput of about 5 m^3/s. [22]

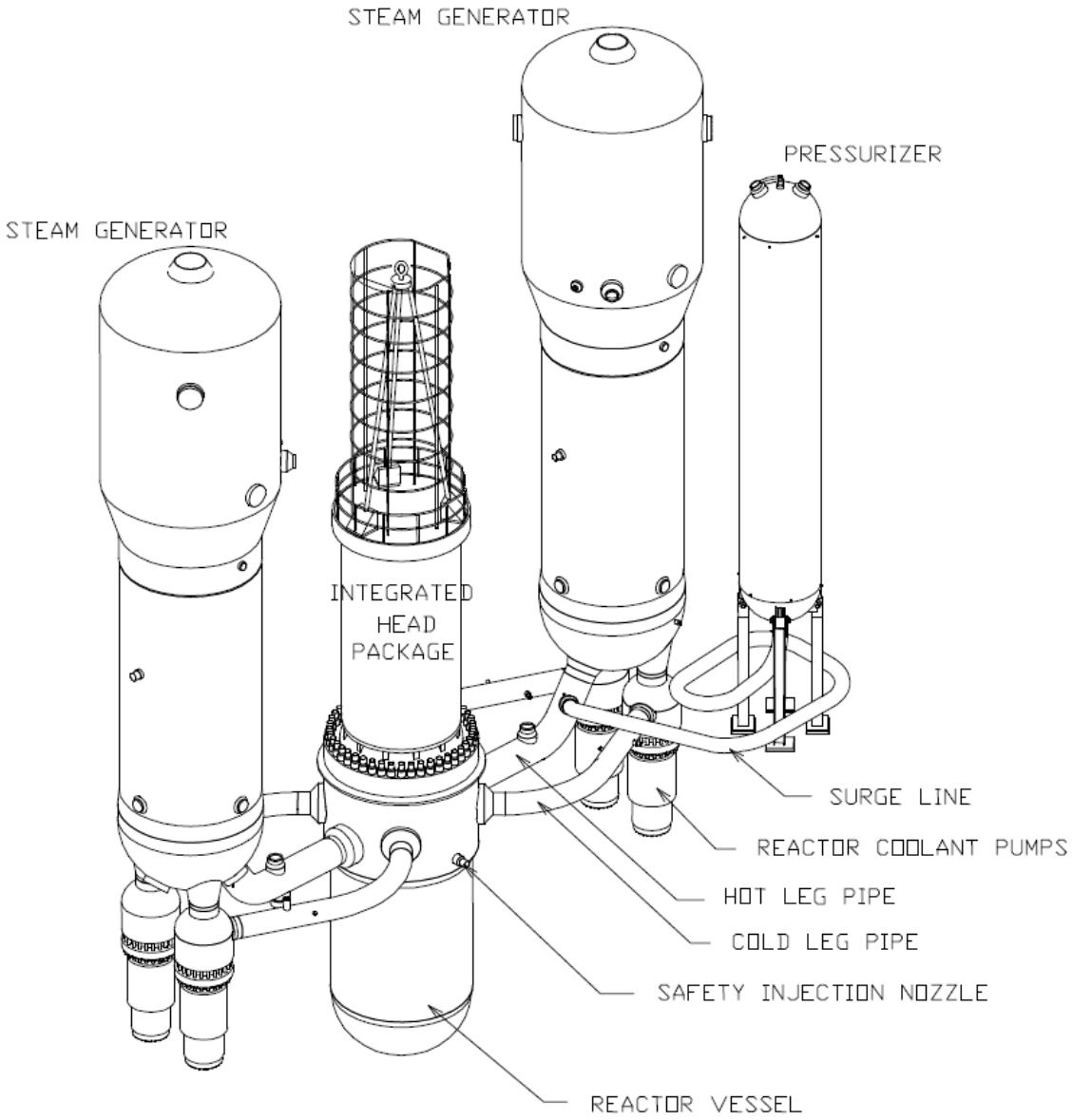

Fig. 26: AP1000 Primary Circuit [23]

4. Neutron Transportation

Chapter 2.3.5 explained the general condition for criticality. As mentioned, Eq. 2.17 is only valid for an infinitely extended, homogeneous arrangement. Although the extension by non-leakage-probability factors for fast and thermal neutrons takes into account the finite size of an actual reactor, it continues to assume a homogeneous distribution of the different components in the reactor. For real arrangements, this simplified calculation for the description of neutron behavior is not sufficient, the description of the spatial, energetic and temporal neutron distribution is generally necessary.

In the following the derivation of the Neutron-Boltzmann-Equation, also called the neutron transport equation, which describes the underlying problem of neutron transport, is explained. Furthermore, the Monte-Carlo method used for this thesis is described in more detail.

4.1 Neutron-Boltzmann-Equation

The path of an individual neutron can not be predicted precisely, its motion is called Brownian motion or random walk. At any point where speed and/or direction change, a collision with an atomic nucleus takes place. The length between two collisions depends on the mean free path, which in turn depends on the macroscopic cross-section according to Eq. 4.1.

$$\lambda = \frac{1}{\Sigma} = \frac{1}{\sigma \cdot N} \tag{4.1}$$

These collisions lead to a redistribution of the neutrons. This process is called diffusion. In contrast to the diffusion of gases, however, neutron-neutron interaction can be neglected due to the low neutron density compared to the atomic density. Neutrons are assumed to only interact with atomic nuclei.

To describe the motion of a single neutron, seven independent variables are necessary: three each to describe the location and direction of the neutron, and one to describe the motion's time dependence. For practical reasons, the direction of the neutron is divided into the kinetic energy E and the direction $\vec{\Omega}$ in spherical coordinates.

The six components of the location and velocity vectors $\vec{r}$, $\vec{\Omega}$ and E span the so-called

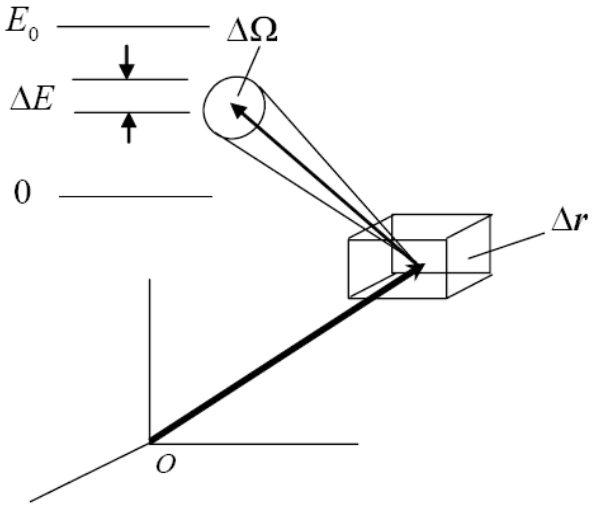

Fig. 27: Phase space element [24]

phase space. Each point in the phase space describes all neutrons at the location $\vec{r}$ with energy E and direction $\vec{\Omega}$. The differential volume of a phase space element is described through

$$\Delta q = \Delta E \Delta \vec{\Omega} \Delta V. \tag{4.2}$$

A graphic representation of the phase space element is given in Fig. 27. Furthermore, the neutron density distribution $N(\vec{r}, \vec{\Omega}, E, t)$ can be described. It can be used to define another important quantity, the neutron flux, with v being the neutron velocity.

$$\phi(\vec{r}, \vec{\Omega}, E, t) = vN(\vec{r}, \vec{\Omega}, E, t) \tag{4.3}$$

Additionally, the neutron current vector represents the directed neutron flux in the direction $\vec{\Omega}$ and is defined as follows:

$$\vec{J}(\vec{r}, \vec{\Omega}, E, t) = \vec{\Omega}\phi(\vec{r}, \vec{\Omega}, E, t) \tag{4.4}$$

With the macroscopic cross-section Σ and the neutron flux, the reaction rate in a single phase space element Δq can be determined:

$$\text{Reaction Rate} = \Sigma(\vec{r}, E, t)\phi(\vec{r}, \vec{\Omega}, E, t)\Delta q. \tag{4.5}$$

While the direction of the incident neutron is not relevant for the macroscopic cross-section, it has to be taken into account for scattering processes, since the angle between the incoming and outgoing direction of the scattered neutron determines the energy loss of the neutron. The macroscopic scattering cross-section for a scattering angle between incident ($\vec{\Omega}'$) and outgoing ($\vec{\Omega}$) neutron is given by Eq. 4.6.

$$\Sigma_s(\vec{r}, \vec{\Omega}' \cdot \vec{\Omega}, E' \to E, t) = \Sigma_s(\vec{r}, E', t) \cdot f_s(\vec{\Omega}' \cdot \vec{\Omega}, E' \to E) \tag{4.6}$$

The second term in the equation describes the probability for a collision from the direction $\vec{\Omega}'$ with energy E' into the solid angle $\Delta\Omega$ and the energy range ΔE. The term must also satisfy the normalization

$$\int_0^\infty dE \int_{4\pi} d\vec{\Omega} f_s(\vec{\Omega}' \cdot \vec{\Omega}, E' \to E) = 1. \tag{4.7}$$

In order to be able to formulate the Boltzmann-equation for neutrons, with which the neutron distribution can be calculated, the neutron gains and losses in the phase space element dq are compared per unit of time. These are explained in more detail below.

Losses

- *Absorption*
  It is obvious that absorption reduces the number of neutrons. This term contains all absorption processes, including those inducing fission in the target nucleus.

$$\text{Absorption Losses} = \Delta\vec{\Omega}\Delta E \int_V d\vec{r}\, \Sigma_a(\vec{r}, E, t)\phi(\vec{r}, \vec{\Omega}, E, t) \tag{4.8}$$

- *Scattering*
  Neutrons are lost also by scattering. Every neutron that scatters in the phase space element changes direction and/or energy and thus leaves the considered phase space element Δq.

$$\text{Scattering Losses} = \Delta\vec{\Omega}\Delta E \int_V d\vec{r}\, \Sigma_s(\vec{r}, E, t)\phi(\vec{r}, \vec{\Omega}, E, t) \tag{4.9}$$

- *Spatial streaming*
  Furthermore, losses are caused by neutrons streaming out of the volume element

ΔV. These losses are described by the product of neutron current vector and normal vector of the surface of the considered volume. Using the divergence theorem, this area integral can be transformed into a volume integral. In this term, both in- and outflow of neutrons are considered.

$$\text{Streaming Losses} = \Delta\vec{\Omega}\Delta E \int_V d\vec{r}\, \nabla \cdot \vec{J}(\vec{r}, \vec{\Omega}, E, t) \tag{4.10}$$

Gains

- *Scattering*
  Neutrons can also be scattered from another phase space element into the considered Δq. The neutron increase is described by

$$\begin{aligned}\text{Scattering Gains} = \Delta\vec{\Omega}\Delta E \int_V d\vec{r} \int_0^\infty dE' \cdot \\ \int_{4\pi} d\vec{\Omega}' f_s(\vec{\Omega}' \cdot \vec{\Omega}, E' \to E) \Sigma_s(\vec{r}, E', t) \phi(\vec{r}, \vec{\Omega}', E', t).\end{aligned} \tag{4.11}$$

- *Fission Neutrons*
  Neutrons released by fission also increase to number of neutrons. The number of fissions per Δt is represented by

$$\text{Number of Fissions} = \int_V d\vec{r}\, \Sigma_f(\vec{r}, E', t) \phi(\vec{r}, \vec{\Omega}', E', t) dE' d\vec{\Omega}'. \tag{4.12}$$

  The proportion of these neutrons in the phase space element Δq is thereby

$$\text{Fission Neutrons in } \Delta\vec{\Omega}\Delta E = \frac{\chi(E)}{4\pi} \nu(E') \Delta\vec{\Omega}\Delta E. \tag{4.13}$$

  The term $\chi(E)$ can be taken from Eq. 2.13, $\nu(E)$ represents the average number of fission neutrons per fission process. This results in the total neutron gain from fission in $V\Delta\vec{\Omega}\Delta E$ per Δt:

$$\begin{aligned}\text{Fission Gains} = \Delta\vec{\Omega}\Delta E \int_V d\vec{r}\, \frac{\chi(E)}{4\pi} \int_0^\infty dE' \cdot \\ \int_{4\pi} d\vec{\Omega}'\, \nu(E') \Sigma_f(\vec{r}, E', t) \phi(\vec{r}, \vec{\Omega}', E', t).\end{aligned} \tag{4.14}$$

- *Neutron Sources*
  Neutron sources that emit neutrons into the phase space element Δq also contribute to the neutron balance.

$$\text{Neutron Source Gains} = S(\vec{r}, \vec{\Omega}, E, t)\Delta q \tag{4.15}$$

The temporal changes of the neutron density can thus be composed of the individual terms to the Neutron-Boltzmann-Equation. Absorption and scattering are both represented by the total macroscopic cross-section Σ. As the equation has to be valid for every chosen volume, the equation can be expressed as follows. [24]

$$\begin{aligned}
&\left[\frac{1}{v}\frac{\partial}{\partial t} + \vec{\Omega}\cdot\nabla + \Sigma(\vec{r}, E, t)\right]\phi(\vec{r}, \vec{\Omega}, E, t) = \\
&= \int_0^\infty dE' \int_{4\pi} d\vec{\Omega}\Sigma_s(\vec{r}, \vec{\Omega'}\cdot\vec{\Omega}, E' \to E)\phi(\vec{r}, \vec{\Omega}, E, t) + \\
&+ \frac{\chi(E)}{4\pi}\int_0^\infty dE' \int_{4\pi} d\vec{\Omega'}\nu(E')\Sigma_f(\vec{r}, E', t)\phi(\vec{r}, \vec{\Omega}, E, t) + S(\vec{r}, \vec{\Omega}, E, t)
\end{aligned} \tag{4.16}$$

This equation is the basis of the calculation of neutron transport. However, it is not completely solvable in this form. In order to solve them analytically, different simplifications and approximations have to be applied. On the one hand, discretizations of the different approximation methods cause systematic errors in the calculation of neutron transport. On the other hand, for most approximation methods, it is not possible to calculate three-dimensional configurations properly. The consequent restriction to one- or two-dimensional configurations leads to further errors.

4.2 Monte-Carlo Method

Another way to solve equation 4.16 respectively the underlying problem is the Monte-Carlo method, which is a purely statistical method. Basically, the Monte-Carlo method is based on simulating several so-called particle histories. For each history, a random game is played with a single particle. The outcome of such a particle history is determined by using a combination of a set of random numbers and physical probabilities of occurrence of the various events. The course of each particle is tracked and recorded. To get a better understanding of how the Monte-Carlo method works, we will have a look at a simple example.

A single neutron history starts with the generation of the neutron. The starting position, energy and direction are determined by the source definition. This for example can be a monoenergetic source with a defined emission direction, but can also be a source with different energies and directions, for example a fission process. If the latter is the case, the start parameters are determined with the help of random numbers and the probability distributions corresponding to the source. It is then necessary to determine where the generated neutron experiences its first collision. For this calculation, the mean free path length (Eq. 4.1) is used, which depends on the cross-section of the considered material. The collision probability in the interval dr is determined by the distribution function Eq. 4.17 and sampled with another random number.

$$p(r)dr = \Sigma_t e^{-\Sigma_t \cdot r} dr \tag{4.17}$$

In addition, which interaction takes place is determined via the cross-sections for the different individual processes. Considering only the possibility of elastic scattering and absorption, the probabilities for these two processes are Σ_s/Σ_t and Σ_a/Σ_t, respectively. Another random number is created to determine which of the two processes takes place at the collision location. If the neutron is scattered elastically, the scattering angle and thus the energy loss are determined and the history will be continued. In the event that the neutron is absorbed or leaves the volume of interest, the history is terminated and the next neutron is sampled. It should be noted, that this example is greatly simplified. The accuracy of such a simulation depends on the number N of simulated neutron histories. The corresponding stochastic error decreases with $N^{-1/2}$ for the most cases. [25]

Variance Reduction

The requirement for a large number of histories for a sufficiently accurate result gives rise to a separate challenge for models in which only a small proportion of the generated neutrons penetrate into the volume of interest. This is the case, for example, with shielding calculations. In order to keep the number of total runs within a reasonable range and at the same time obtain accurate results, so-called variance reduction methods are used. There is a variety of different methods, in the following, one of these methods used for this thesis is described in more detail.

The variance reduction method *Geometry splitting with Russian roulette* can be used to achieve better statistics in areas of interest. In the case of this method, a neutron reach-

ing an area of higher "importance" gets split. In how many parts the neutron is divided, depends on the ratio of the "importances" of the involved areas. For example, if a neutron enters a region with importance 2, coming from a region with importance 1, the neutron is split into two parts. The subsequent simulation of the two parts then takes place independently of each other. It should be noted that the "weight" of the particle, with which it contributes to the result of the simulation is adjusted accordingly. This method reduces the variance of the result. [25]. Similarly, particles entering a region of lower importance are partially terminated. The termination probability is again dependent on the importance ratio, the weight of the particle is corrected as well.

Tallies

In order to get the desired insight from the simulation, it is necessary to record certain information of the individual particle histories. Of course, the type of information required depends on the problem itself, but in most cases, the information of interest are neutron flux and neutron current. For example, as in this thesis, it is necessary to determine the average neutron flux in a specific volume. This problem can be formulated as

$$\overline{\phi}_V = \frac{1}{V} \int dE \int dV \int d\vec{\Omega} \int dt\, \phi(\vec{r}, \vec{\Omega}, E, t). \tag{4.18}$$

The program MCNP5 used for this work determines the average neutron flux $\overline{\phi}_V$ via the track length T_l, i.e. the time of the neutron in the considered volume multiplied by its velocity, of the individual neutrons. The average neutron flux in the considered volume thus takes the following form for N particles, with W being the individual neutron weight [26]:

$$\overline{\phi}_V = \sum_i^N \frac{W_i \cdot T_{l,i}}{V} \tag{4.19}$$

5. MCNP5 - Model and Calculations

For the calculations performed for this thesis the program MCNP5 (Monte-Carlo N-Particle Code Version 5) was used. This is a general purpose Monte-Carlo transport code, which can be used to calculate the transport of neutrons, photons or electrons, or a combination thereof. Evaluated cross-section data from databases such as ENDF/B-VII are used. The use of continuous-energy nuclear data libraries allows for an exact description of the neutron transport.

In the following, this chapter describes the model for calculating the neutron flux in the area of the reactor pressure vessel as well as the model used to evaluate the neutron spectrum for the source used. The results of these calculations are described in Chapter 6.

5.1 Model RPV

In the first step of using MCNP, it is important to choose a model for the calculations that describes the underlying problem with sufficient accuracy. Fig. 28 schematically shows the model of a pressurized water reactors RPV. However, performing any calculations with this model would result in an enormous calculation time per repetition. Moreover, only the neutron flux distribution in the radial direction is of interest for this thesis. Therefore, instead of a complete reactor, a planar model was created. The dimensions of the RPV, its internals and the Biological Shield (BioS) correspond to those of Unit 2 of the Chashma Nuclear Power Plant (CHASNUPP-II). [27]

The model of the RPV includes the following areas:

- Baffle
- Flow Channel (water-filled area between baffle and core barrel)
- Core Barrel
- Downcomer (water-filled area between core barrel and RPV)
- RPV cladding

- RPV
- Air-filled space between RPV and BioS
- Biological Shield

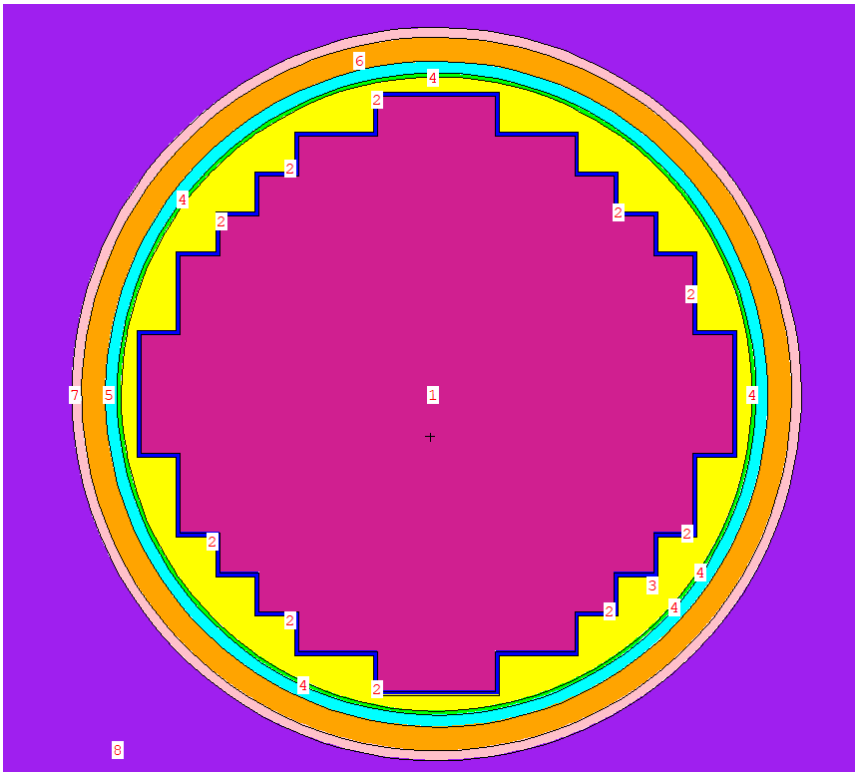

Fig. 28: Cylindrical RPV model

In the first step in creating the model in MCNP, the surfaces confining the individual areas are defined. In general, MCNP uses first- and second-degree surfaces and so-called macrobodies. [26] In this case the geometry is relatively simple, for the different areas adjacent parallelepipeds are used.

Furthermore, the *mode* is defined, which determines for which particle type the program performs the transport calculation. In this case, one is only interested in neutron transport, which is why *mode n* is chosen.

In the next step, the materials of the individual areas are determined. For the individual materials, the elements contained are given proportionally. The *ZZZAAA* format

is used to indicate certain isotopes, the first three digits indicate the atomic number, the last three indicate the mass number. Using *000* instead of the mass number, the natural isotope distribution can be used for an element for material definition. Furthermore, by specifying a particular cross-section library, on the one hand the temperature of the material can be given, which leads to the consideration of cross-section Doppler broadening, on the other hand it can be defined whether continuous or discrete data sets are to be used.

Furthermore, the S(α,β) material card states that in this case, for material 1, water, beneath a certain neutron energy, typically 4 eV, the free gas model should no longer be used. Instead, the scattering function S(q,ω) or S(α,β) derived from thermal neutron scattering theory is used, which takes into account the thermal motion of the target nuclei and chemical bonding effects. In this case, this increases accuracy for neutron moderation in water. The proportion of the various elements or isotopes can be stated either with respect to the atomic or weight proportion. The following materials are defined for the calculations: [28], [29]

- Water
- AISI Type 304 stainless steel
- ASTM A533 low alloy steel
- Ordinary concrete
- Boron-carbide doped concrete
- Cadmium
- Air

After surfaces and materials are described, the corresponding cells are defined. For this purpose, the boundary surfaces, material of the cell and the temperature-dependent density of the material are given. In addition, the neutron importance is determined. As a result, on the one hand the considered volume can be limited. Neutrons entering a cell of importance zero are terminated and their history end. On the other hand, importance is used for variance reduction methods (see Chapter 4.2). In this case, the RPV is divided into 5 single cells, with each cell increasing the neutron importance by a factor of two. This increases the number of events in the areas further from the source.

Furthermore, it is necessary to specify a neutron source. In order to minimize the computation time per experiment, source calculation is performed separately. The result of this calculation is then implemented as directed area source in positive x-direction in the RPV model at the boundary between core and baffle plate. A description of the source model and results can be found in Chapter 5.2 and 6.1.

In addition, the tallies are given for the model. In this case, one is interested in the neutron flux, especially in the area of the RPV. For this purpose, a mesh tally was placed upon the desired area, which extends from the middle of the downcomer to half of the BioS. In the y- and z-direction, the mesh lies in the center of the defined geometry. The tally consists of 150 equal segments, which allows for a spatial resolution of the neutron flux in the x-direction. In this case, the segment size should be selected so that on the one hand the spatial resolution is sufficiently high, on the other hand the number of events occurring in each segment is large enough to minimize the statistical error. For the RPV model, the size of a single segment was set to 0.97 x 20 x 20 cm. The mesh-tally is further divided into energy ranges of 0 - 200 meV, 200 meV - 10 keV and 10 keV - 10 MeV, i.e. thermal, epithermal and fast neutrons.

Finally, the number of simulated neutron histories is determined by means of the NPS card. While more iterations improves the statistic of the result, they increase the calculation time, so a balance has to be found. For this thesis, the number of neutrons simulated per experiment was 10^9. The model used can be seen in Fig. 29.

5.2 Model Source

In order to obtain the neutron spectrum of a western pressurized water reactor for the source of the RPV model, the decision was made to simulate a single fuel assembly. The model consists of a square 17x17 arrangement, with 25 free spaces for control rods, neutron sources or core instrumentation. The simulated fuel element has a height of 3.64 m and a base area of 20x20 cm. The parameters used for simulation at operating temperature originate from the simulation program PCTRAN [30].

The fuel consists of uranium dioxide pellets, for the simulation of the source an enrichment

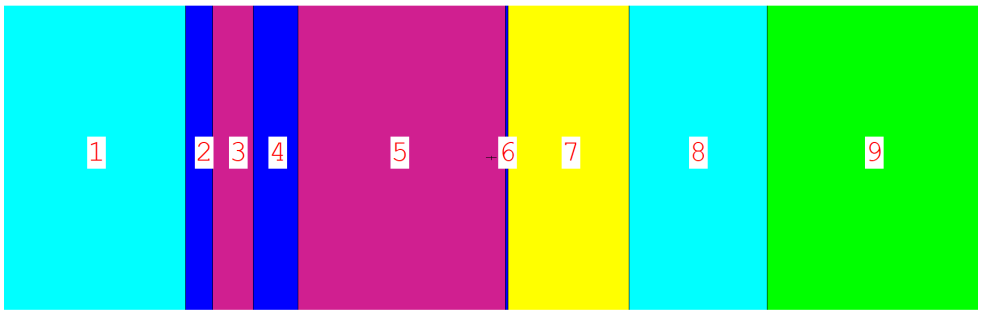

Fig. 29: Illustration of planar model:
1: Core; 2: Baffle Plate; 3: Flow Channel; 4: Core Barrel; 5: Downcomer;
6: RPV Cladding; 7: RPV; 8: Air Gap; 9: Biological Shield

of 4% was chosen. The nuclear fuel is surrounded by a Zircaloy-4 cladding tube, the space between fuel and cladding is filled with helium. The fuel rod is surrounded by water. Fig. 30 shows a closer view of a single fuel rod.

To simulate the source, a single fuel rod is modeled and repeatedly positioned in a grid in the desired arrangement. The creation of the input file is analogous to that of the RPV model. However, in the case of the source model, the outer surfaces of the array are defined as neutron reflective so as to simulate the juxtaposition of multiple fuel elements and hence the effects on each other. For the carried out criticality simulation further start neutrons are needed. For this purpose, a rod-shaped source of ^{252}Cf was chosen, which is positioned in the middle of the fuel assembly. ^{252}Cf has a half-life of 2.6 years and fissions spontaneously with a probability of 3%. [6] In the fission process, 3 to 4 neutrons are released, with a mean neutron energy of 2.3 MeV. [26] Fig. 32 shows the fission neutrons energy spectra for ^{235}U and ^{252}Cf. Fig. 31 shows the starting neutrons in the fuel assembly model. Due to the similar energy distribution and high neutron yield, ^{252}Cf is used as a starting source in nuclear reactors.

The *kcode* card in the input file defines, that this simulation should be treated as criticality calculation. In contrast to simulations with a fixed source, as in Chapter 5.1, the starting point of the next neutron generation is variable and depends on the location of the fission-

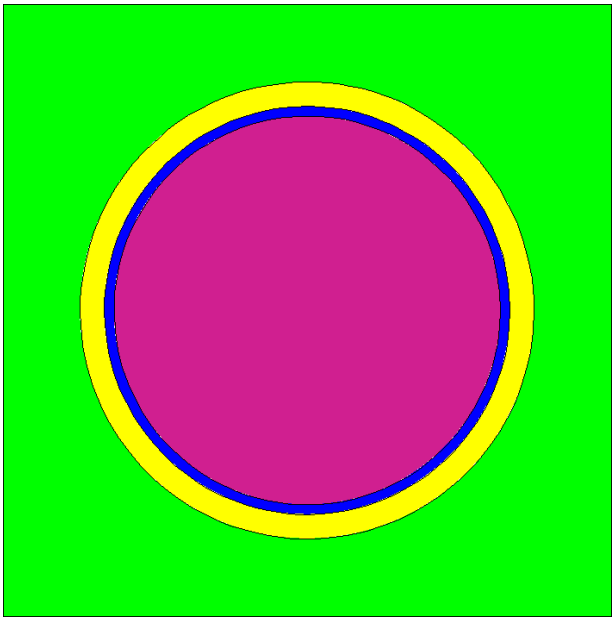

Fig. 30: Fuel rod model

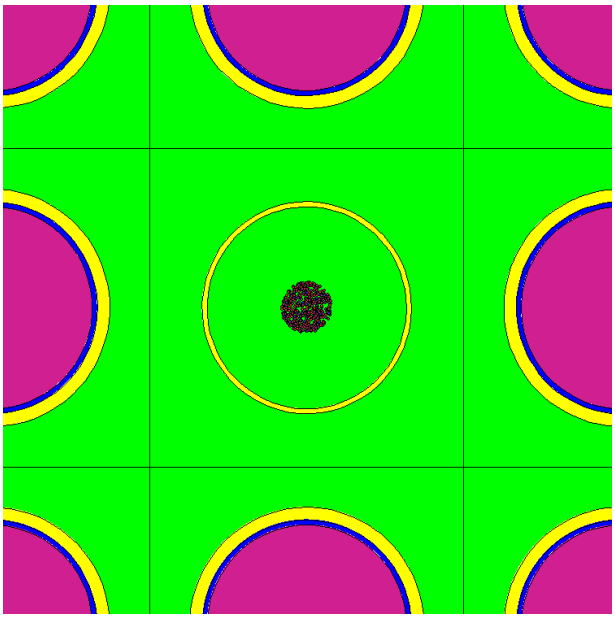

Fig. 31: ^{252}Cf starting neutrons

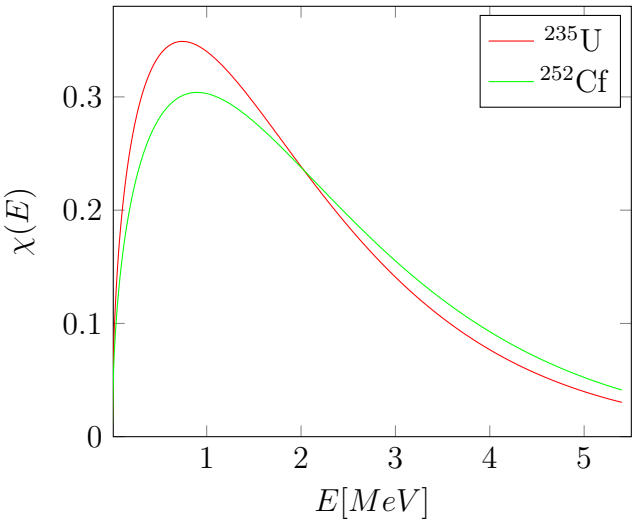

Fig. 32: Fission neutron energy spectra for ^{235}U and ^{252}Cf [26]

inducing absorption of the previous generation. This is a very simplified description, for further information reference is made to corresponding literature. To record the energy spectrum of neutrons exiting the fuel element and, consequently, the reactor core, zones filled with air are added around the fuel assembly (cells 10 and 11 in Fig. 33). In cell 11, the energy-resolved neutron flux is recorded.

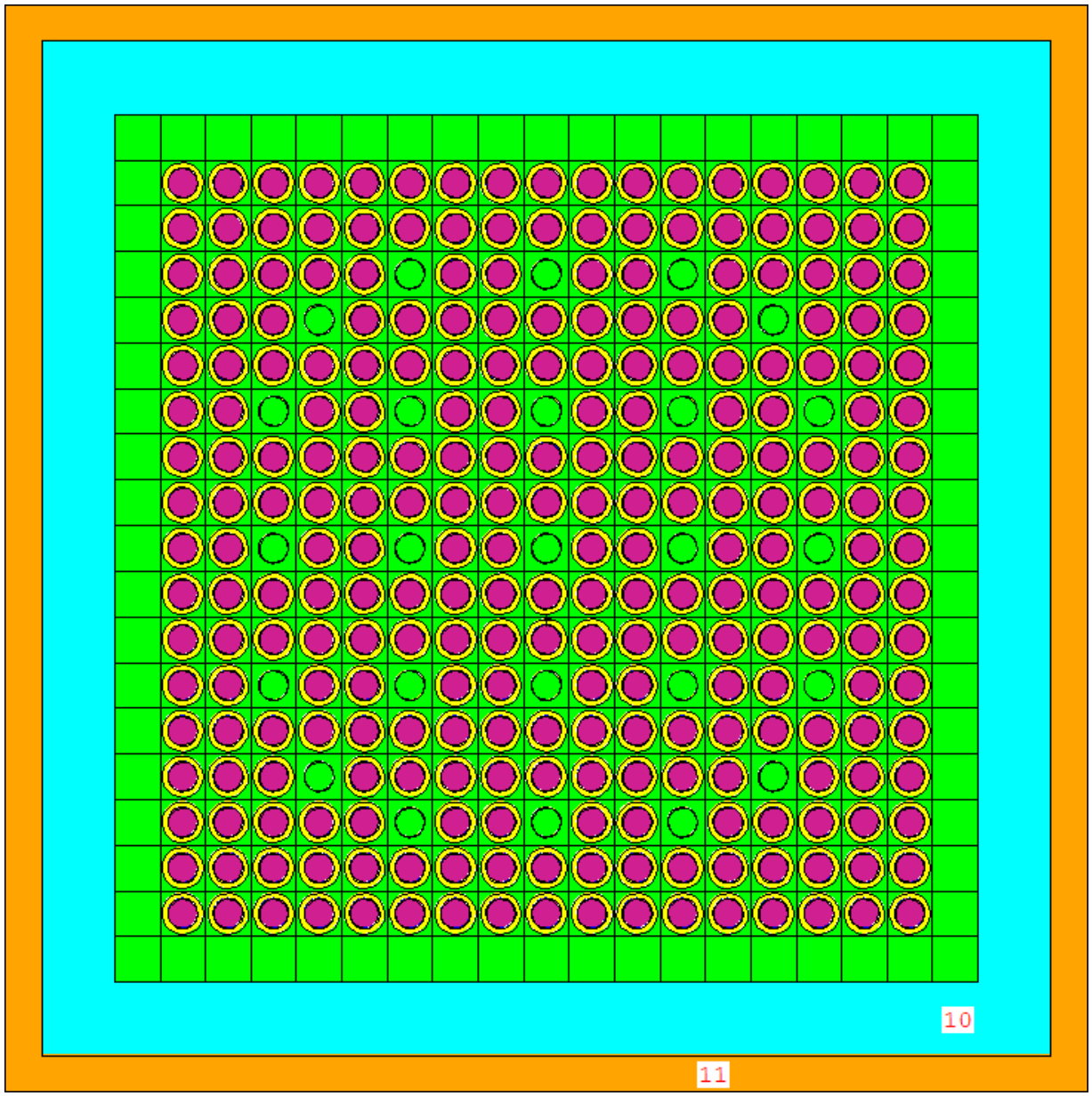

Fig. 33: Fuel assembly model

6. Calculations & Results

This chapter describes the results of the various simulations performed with the models described in Chapter 5.

6.1 Source

The results of the criticality simulations for the fuel element, which where performed both at room temperature and operating temperature, are shown in Fig. 34.

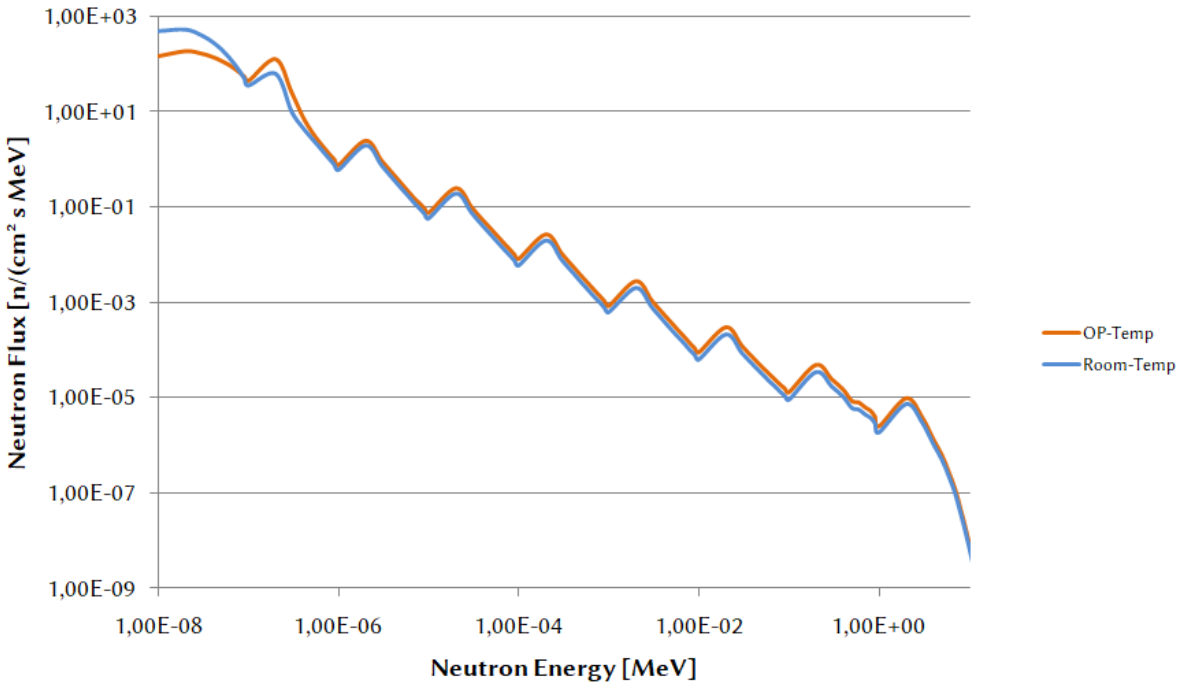

Fig. 34: Fuel element neutron spectra

As can be seen, the neutron spectrum is shifted towards higher energies at operating temperature, the spectrum becomes *harder*. The hardened neutron spectrum results in more neutrons penetrating the core baffle and core barrel. Moderation in flow channel and downcomer result in a higher flux, both in the thermal as well as in the epithermal and fast energy range, in the region within and outside of the RPV. The data shown are then normalized and converted to a surface source. The area source thereby uses the neutron spectrum of the fuel element to determine the initial energy of the generated neutrons. The position of the source in the RPV model can be seen in Fig. 35.

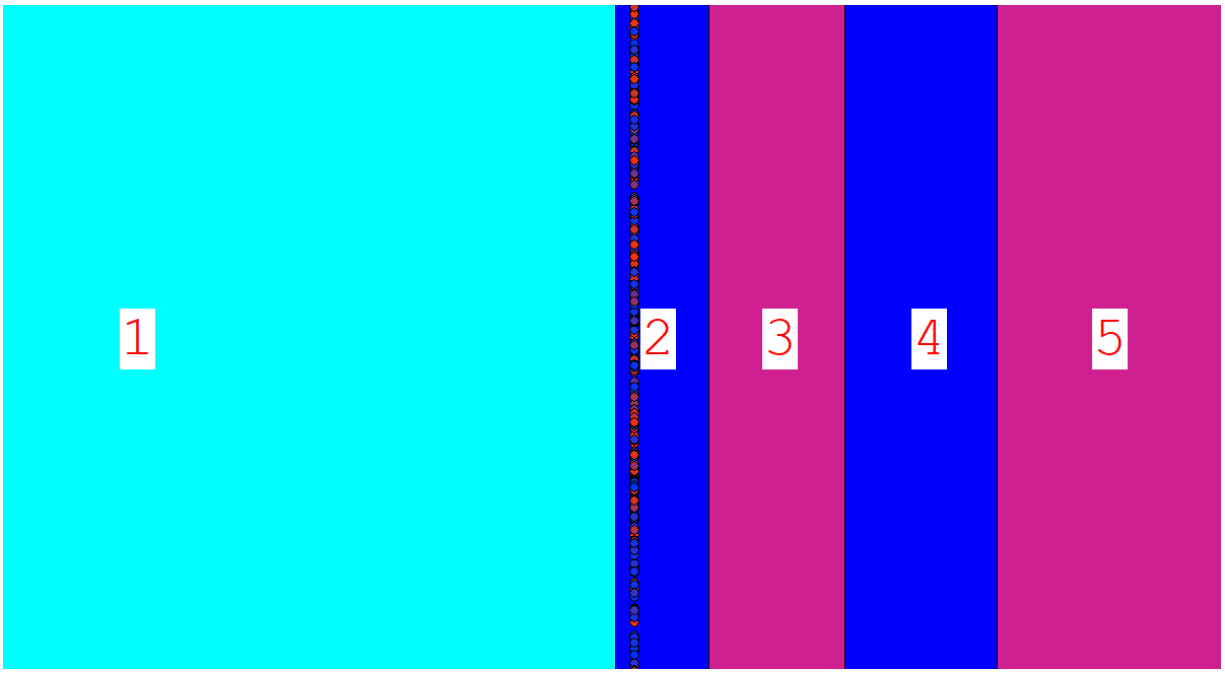

Fig. 35: Source position in model:
1: Core; 2: Baffle Plate; 3: Flow Channel; 4: Core Barrel; 5: Downcomer

6.2 RPV

The first step is to verify that the neutron flux in the region of the RPV, as shown schematically in Fig. 1, can be reproduced using the Monte-Carlo method.

For this the model was simulated as described with 10^9 neutrons, with a processing time of 49.5 hours. The neutron fluence, i.e. neutron flux times time, is normalized to the value at the RPV inside. The result is shown in Fig. 36. To estimate the accuracy of the result the relative error R (Eq. 6.1) is given for each segment of the mesh-tally.

$$R = \frac{1}{\overline{x}} \cdot \frac{1}{N} \cdot \frac{\sum_{i=1}^{N}(x_i - \overline{x})^2}{N-1} \tag{6.1}$$

Based on qualitative analysis and experience, the MCNP manual cites a relative error < 0.10 as a generally reliable result. [26]

For this calculation, this is given for thermal, epithermal and fast neutron flux down to a depth of one meter in the BioS. At this depth, the thermal neutron flux has already

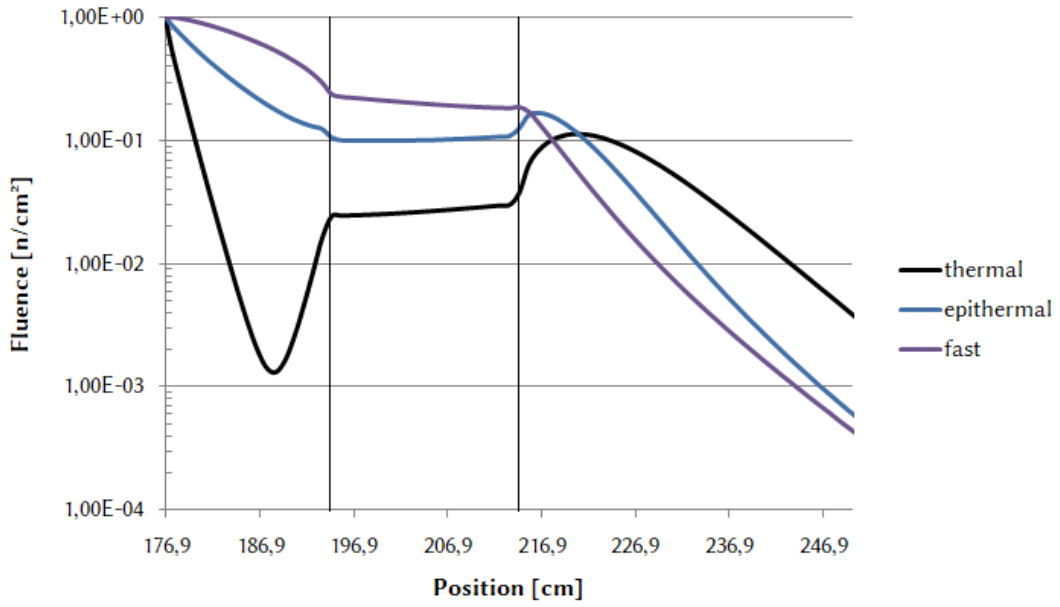

Fig. 36: Thermal, epithermal and fast neutron flux with Biological Shield

dropped six orders of magnitude relative to the RPV inside. One can therefore speak of a reliable result, especially in the area of the RPV. The effects described in Chapter 1 are clearly visible. On the left, the graph is bounded by the inside of the pressure vessel and continues to a depth of half a meter within the BioS. The vertical lines indicate the outer wall of the RPV and the boundary of the BioS.
Coming from the left, i.e. from the reactor side, thermal neutrons enter the pressure vessel and are absorbed successively there. The minimum of the neutron flux in this area is at about 2/3 of the RPV. The flux then increases towards the RPV outside. At the edge it is at about 2% of the inner RPV wall value. The Biological Shield shows very well the formation of a "reservoir" of thermal neutrons. This is, as previously discussed, formed by the thermalization of fast neutrons in the BioS. The epithermal and fast neutron profiles confirm this. The fast neutron flux decreases strongly as it enters the Biological Shield due to the relatively good moderation properties of concrete.

To further verify that the BioS is indeed the source of thermal neutrons responsible for activating the RPV outer wall, the simulation was additionally performed without a biological shield. The result, compared to the one with BioS, is shown in Fig. 37, and further reinforces this assumption.

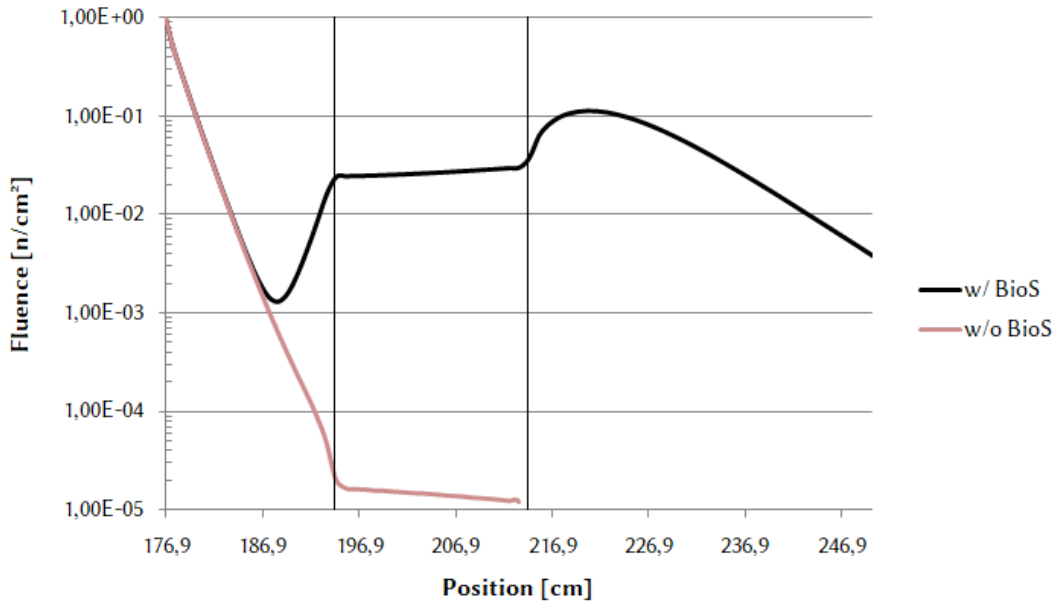

Fig. 37: Thermal neutron flux with & without Biological Shield

In order to reduce the activation of the outer area of the RPV, the two approaches described in Chapter 1 are simulated.

6.2.1 Borated Concrete

The first option for reducing the activation of the outer reactor pressure vessel involves the addition of boron to the concrete of the biological shield. Fig. 3 shows the cross-sections for ^{10}B and ^{11}B for different interaction types. As can be seen, the cross-section for (n,α)-reaction of ^{10}B, especially in the thermal neutron range, is considerably high. The cross-section is about 3,840$\cdot$ 10^{-24} cm^2, for natural isotope distribution it is about 770$\cdot$ 10^{-24} cm^2. Boron is implemented into the Biological Shield in the form of boron carbide (B_4C) as an additive. To study the effects of boron carbide in the BioS on the neutron flux, simulations were carried out for 1 to 5 wt% boron.

Fig. 38 shows the neutron flux profile for 1 wt% boron compared to conventional concrete. One can clearly see the reduction of the thermal "neutron reservoir" in the area of the Biological Shield and thus the reduced thermal neutron flux in the outer area of the pressure vessel.

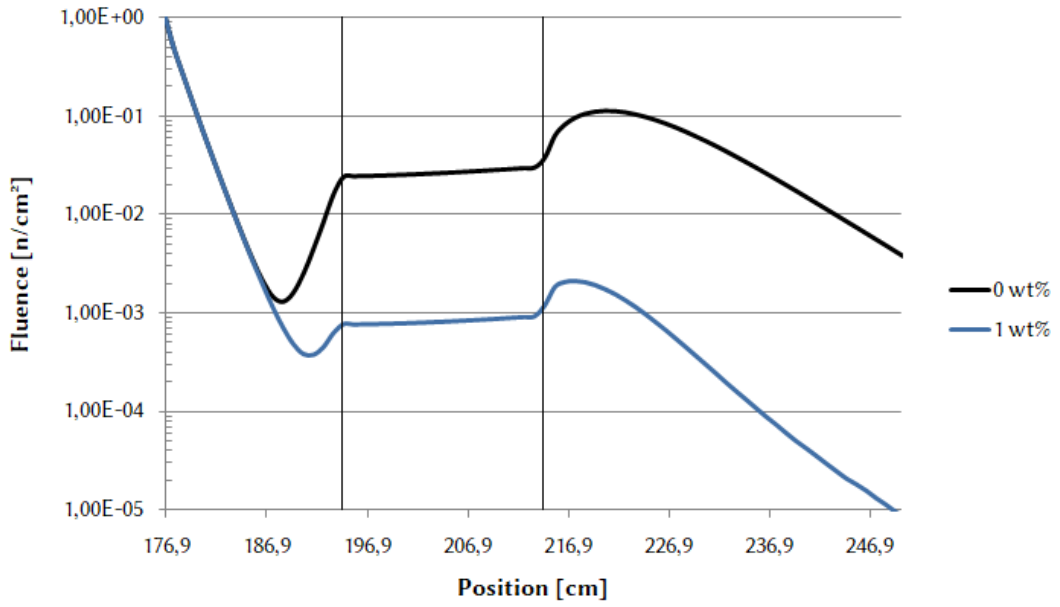

Fig. 38: Thermal neutron flux for 1 wt% boron compared to ordinary concrete

The influence of "boron-doping" of the BioS on the neutron flux in the higher energy ranges can be seen in Fig. 39 and Fig. 40. It is clearly visible that neither the epithermal nor the fast neutron flux are significantly altered. This can be explained by the absorption cross-section of boron, which is orders of magnitude lower in these energy ranges.

Increasing the proportion by weight of boron, the effect is even clearer. The influence of the different boron contents is shown in Fig. 41 for the whole area and in Fig. 42 for the area of the RPV.

Over the entire pressure vessel area, depending on the boron concentration, this measure reduced the thermal neutron flux by only 2.25 to 2.35%, due to the fact that the majority of the thermal neutron flux is located at the inner layers of the RPV. However, considering the area after the neutron minimum of the undisturbed neutron flux, which is located about 12 cm into the RPV, the addition of boron to the BioS leads to a reduction of the thermal neutron flux of 93.5 to 97%. The results for the individual simulations are listed in Tab. 4.

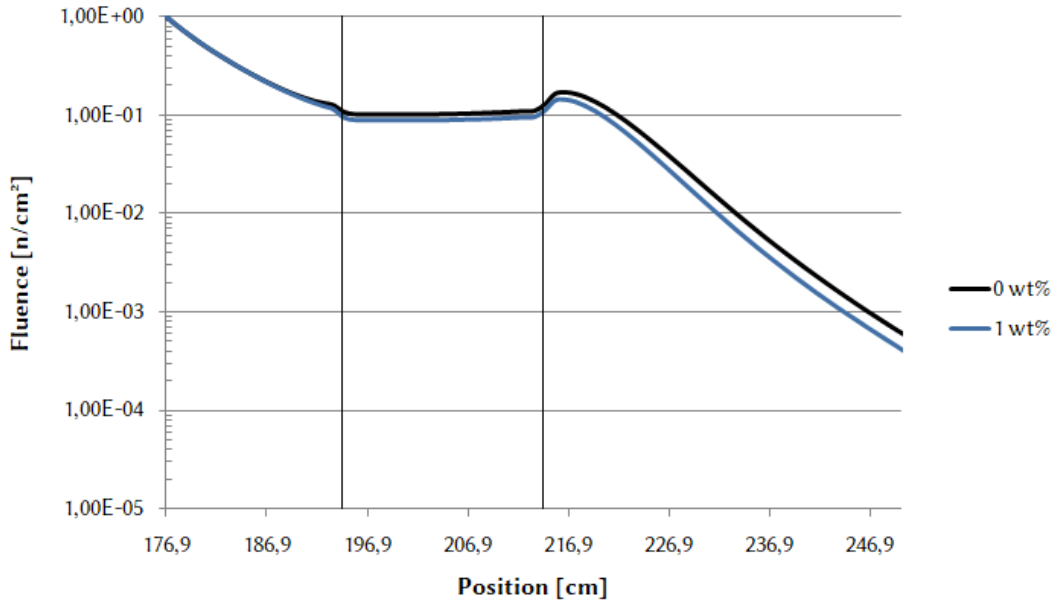

Fig. 39: Epithermal neutron flux for 1 wt% boron compared to ordinary concrete

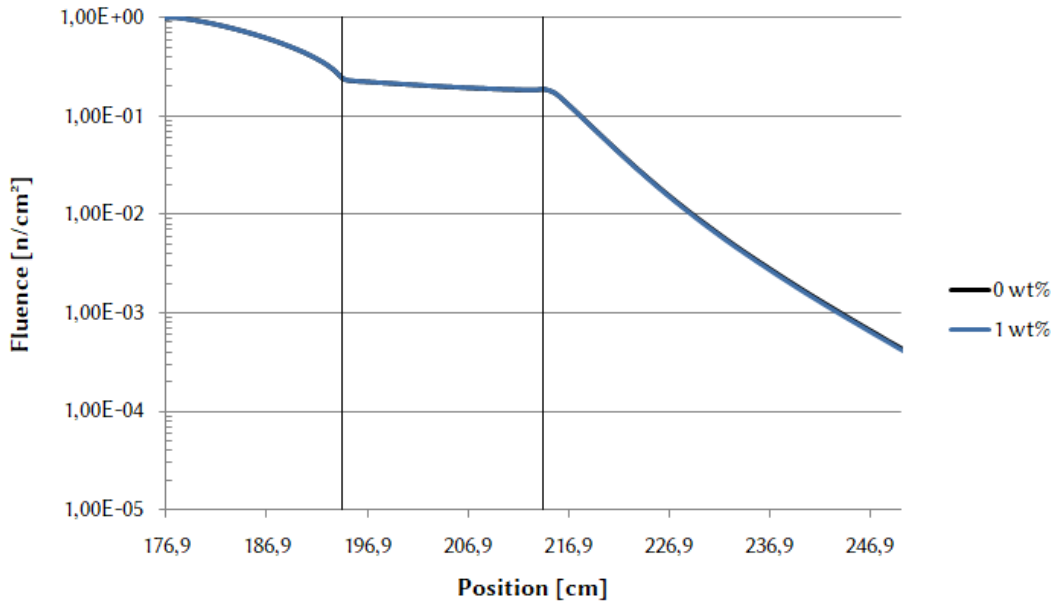

Fig. 40: Fast neutron flux for 1 wt% boron compared to ordinary concrete

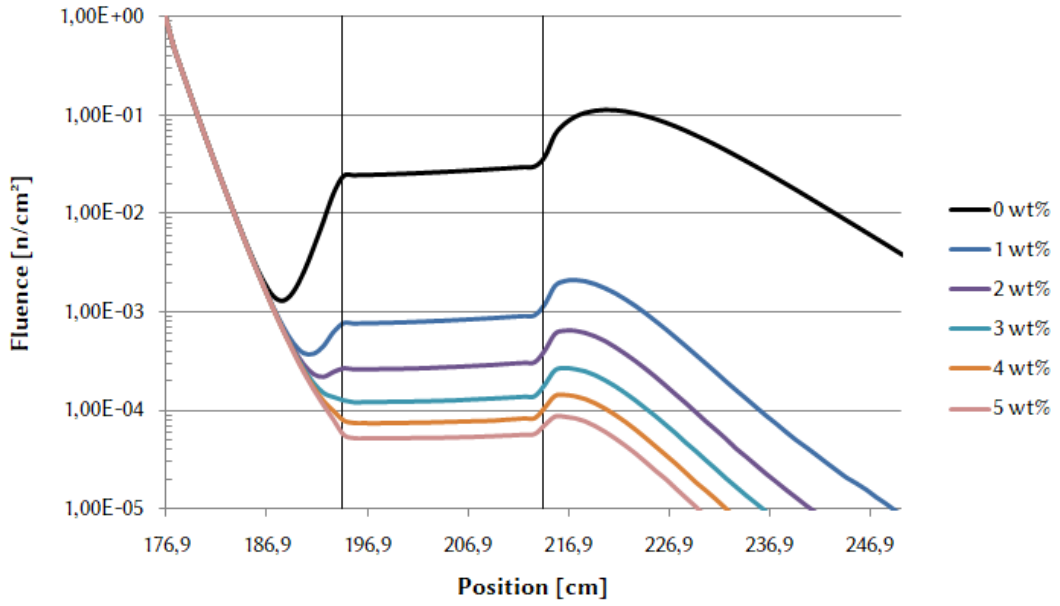

Fig. 41: Thermal neutron flux for different wt% boron

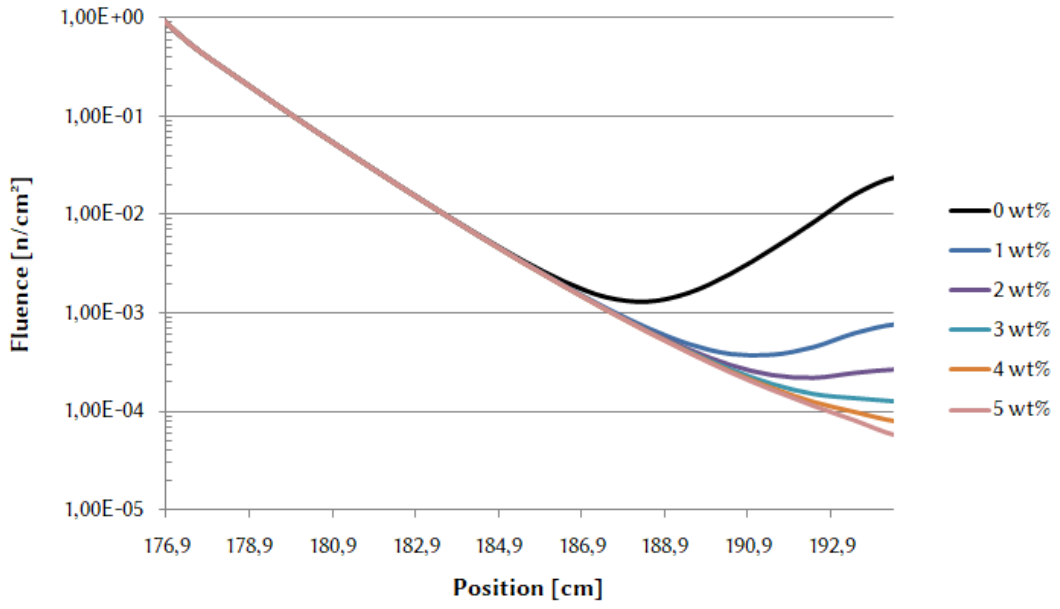

Fig. 42: Thermal neutron flux for different wt% boron over the RPV area

	Reduction total	Reduction after Min.
1 wt%	2.25%	93.52%
2 wt%	2.32%	95.96%
3 wt%	2.33%	96.69%
4 wt%	2.35%	96.96%
5 wt%	2.35%	97.08%

Tab. 4: Neutron flux reduction for different boron concentrations

Furthermore, the simulation for 5 wt% boron content was also carried out at operating temperatures. As described in Chapter 6.1, the parameters changed due to the higher temperatures result in a generally increased neutron flux, but the reducing effect remains (Fig. 43).

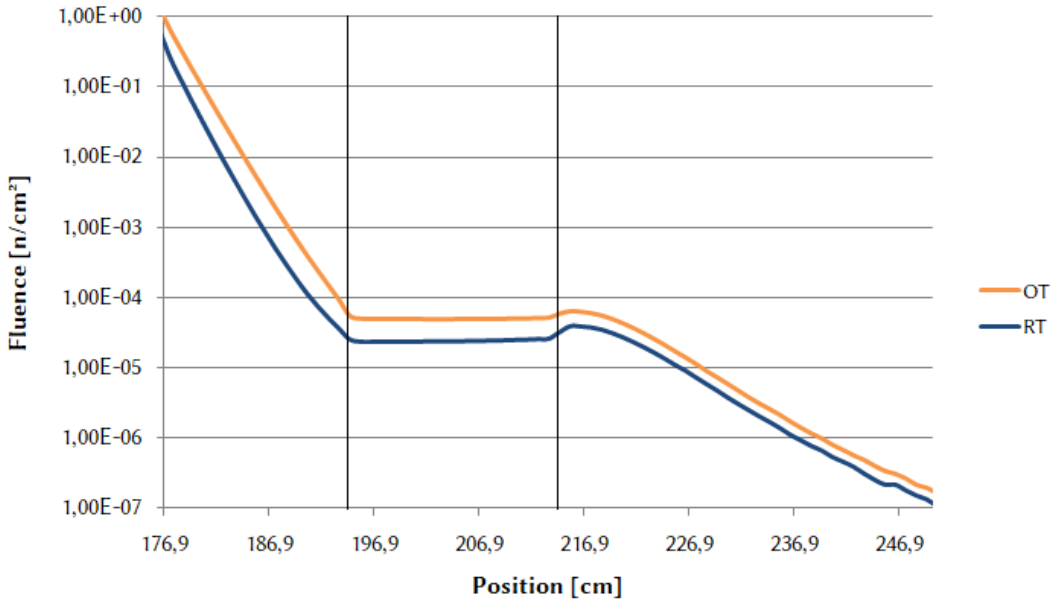

Fig. 43: Neutron flux for 5 wt% at room and operating temperatures

6.2.2 Cadmium Cladding

The second option to reduce the neutron flux in the RPV region is to attach a cadmium cladding to the inside of the Biological Shield. Again, cadmium consists of several naturally occurring isotopes, the isotope of interest for this thesis is ^{113}Cd. As can be seen in Fig. 44,

the cross-section of ^{113}Cd in the thermal neutron range is about 20,000 barn, for natural isotope distribution it is about 2,500 barn.

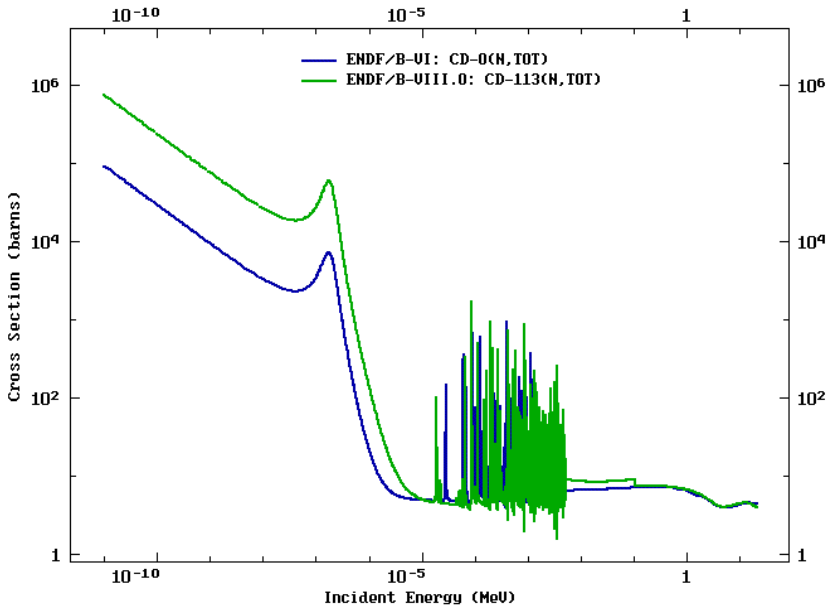

Fig. 44: Total cross-section for natural Cd and ^{113}Cd [6]

The cadmium plates are attached to the inside of the Biological Shield. Cadmium layer thicknesses of 1-3 mm were simulated. Whereas seeding the BioS with boron results in both neutron moderation and absorption within the Biological Shield, moderation and absorption occur spatially separated with this method (Fig. 45). The "neutron reservoir" is still present as with the standard concrete shield, but as soon as thermal neutrons leave the Biological Shield in the direction of the RPV, they are absorbed by the cadmium layer.

As can be seen in Fig. 46 and 47, the influence on the neutron flux, as in the first variant, is limited on the thermal neutron flux, epithermal and fast flux are not affected.

Increasing the layer thickness practically has no additional effect on the neutron flux profile (Fig. 48). A comparison of the simulation data for the cadmium-coated BioS with those without Biological Shield shows that the cadmium layer virtually eliminates any thermal neutron backflow. While the influence on the thermal neutron flux over the entire pressure vessel, as in variant 1, is quite low with a reduction of 2.3%, the flux reduction in the outer RPV region with a layer thickness of 1 mm is already 97%. Increasing the

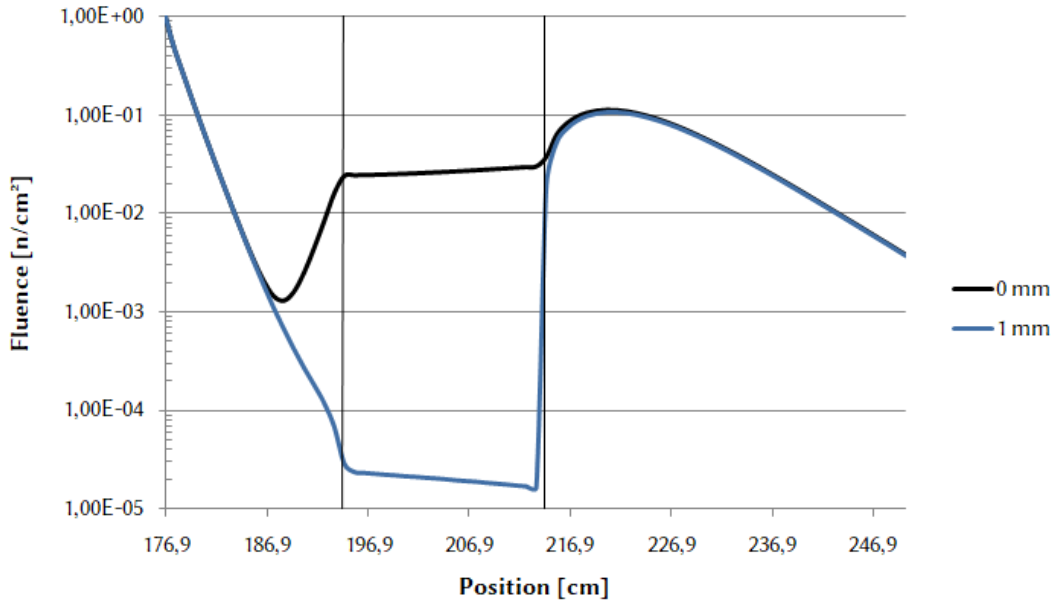

Fig. 45: Thermal neutron flux for 1 mm cadmium cladding compared to standard shield

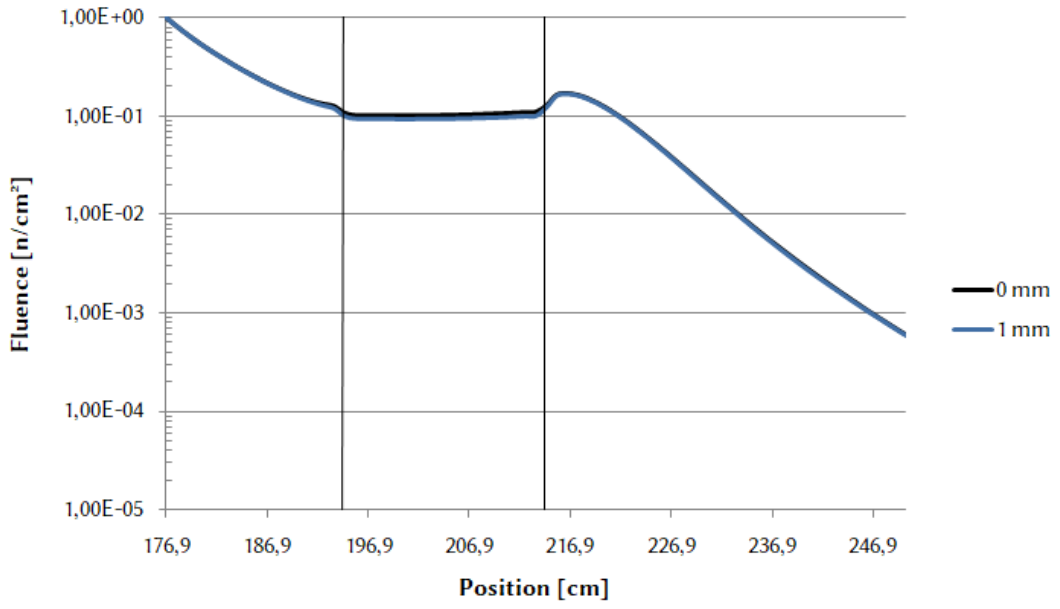

Fig. 46: Epithermal neutron flux for 1 mm cadmium cladding compared to standard shield

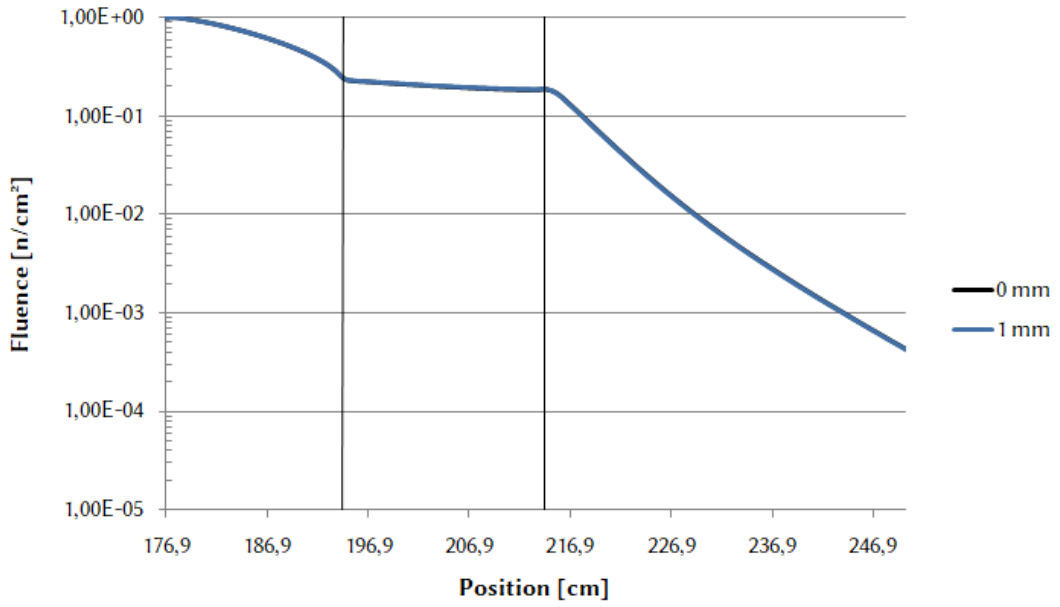

Fig. 47: Fast neutron flux for 1 mm cadmium cladding compared to standard shield

	Reduction total	Reduction after Min.
1 mm	2.33%	97.01%
2 mm	2.34%	97.09%
3 mm	2.35%	97.14%

Tab. 5: Neutron flux reduction for different Cd cladding thicknesses

cladding thickness from 1 to 3 mm further reduces the thermal flux only by about 0.1%. The results of the simulations can be found in Tab. 5. The calculation for a cadmium cladding thickness of 3 mm was also performed at operating temperatures. As with variant 1, the total neutron flux is also slightly higher, but the effect remains the same (Fig. 49).

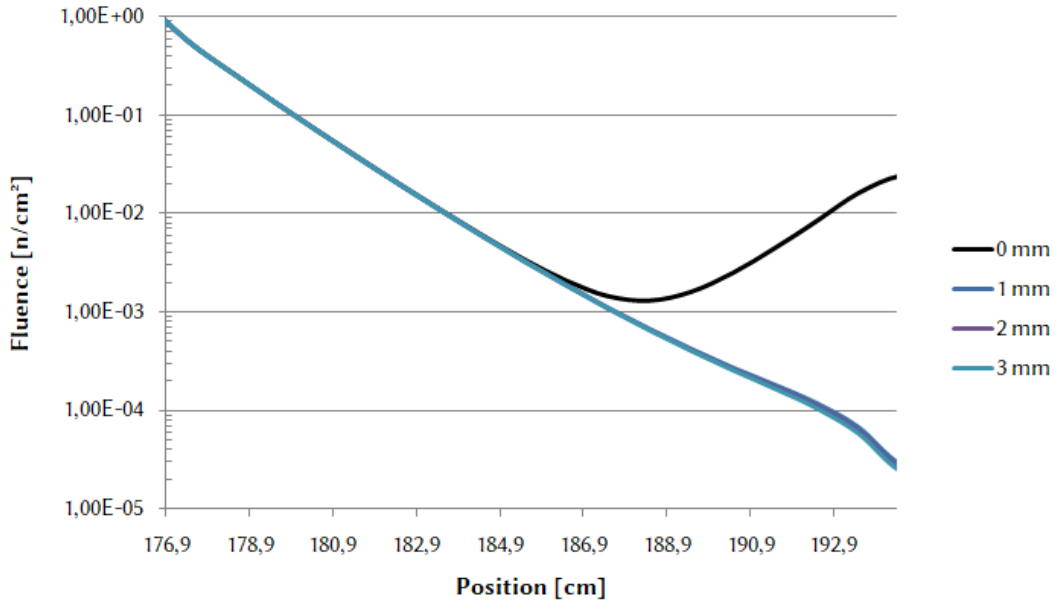

Fig. 48: Thermal neutron flux for different Cd thicknesses in the RPV region

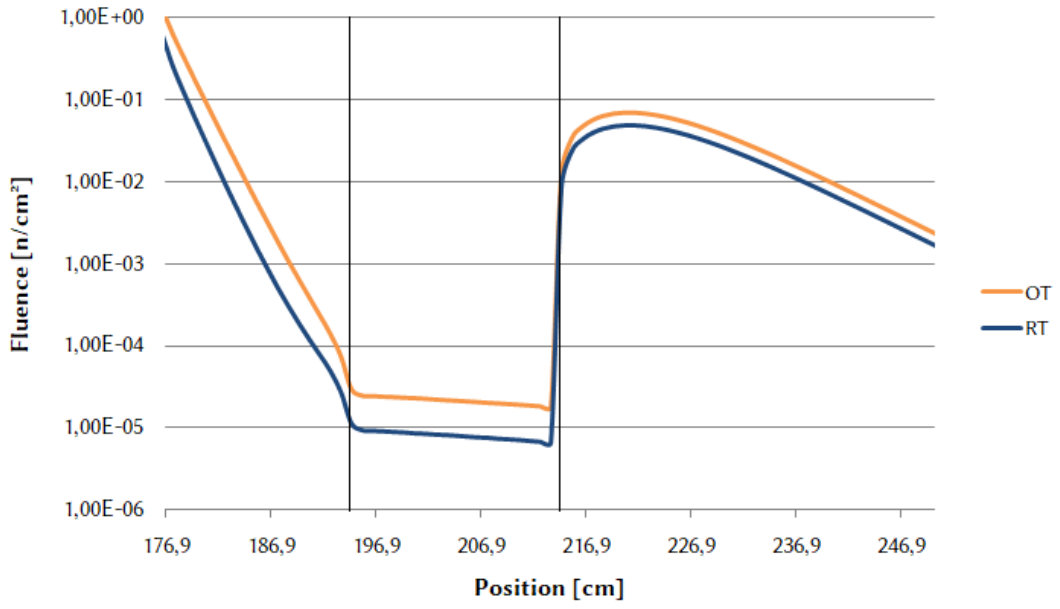

Fig. 49: Thermal neutron flux for 3 mm Cd cladding at room and operating temperatures

7. Summary

The results of the Monte-Carlo calculations show that the thermal neutron flux in the outer area of the RPV can be significantly reduced by the measures described. Although the reduction of the thermal neutron flux over the entire reactor pressure vessel is only in the range of a few percent, the reduction mainly takes place in a sensitive area. Since the outside of the RPV is basically not accessible, especially for large machinery, the neutron flux reduction and thus also the reduction of the total activation brings decisive advantages. For example, with a combination of the above described measures and mechanical removal of the RPV inside the dose rate, emanating from the pressure vessel, could be drastically reduced. Assuming that neutron activation of power plant components is one of the main reasons for long delays in decommissioning a nuclear power plant, the timeframe for decommissioning could be significantly reduced.

However, there are further points of consideration for effective implementation of the described activation reducing measures. When seeding the BioS with ^{10}B, α-particles released in the (n,α)-reaction cause temperature increase in the Biological Shield, which may have an influence on the physical properties of the concrete. Furthermore, the addition of boron carbide to the BioS concrete causes a change in the mechanical properties. Although studies suggest that these changes are negligible at low boron carbide contents, additional research is necessary [31]. When plating the BioS with cadmium, temperature stability of cadmium must be taken into account. Prevailing temperatures between RPV and BioS in combination with the low melting point of cadmium require further in-depth investigation.

List of References

[1] Nuclear Energy Institute. *Decommissioning Nuclear Power Plants*. URL: https://www.nei.org/resources/fact-sheets/decommissioning-nuclear-power-plants.

[2] Anas Gul et al. "Monte Carlo based radial shield design of a typical PWR". In: *ATW-international journal for nuclear power* 62 (Apr. 2017).

[3] Walter Binner. "Reducing neutron activation to support early dismantling of light water reactors". In: *Nuclear Engineering and Design 259* (2013).

[4] M.J. Berger and J.H. Hubbell. *XCOM: Photon Cross Section Database (Version 1.5)*. 2018. URL: http://physics.nist.gov/xcom.

[5] National Institute of Standards and Technology. *Fundamental Physical Constants*. 2019. URL: https://physics.nist.gov/cgi-bin/cuu/Value?mn%7Csearch_for=neutron.

[6] David A Brown et al. "ENDF/B-VIII. 0: The 8 th Major Release of the Nuclear Reaction Data Library with CIELO-project Cross Sections, New Standards and Thermal Scattering Data". In: *Nuclear Data Sheets* (2018).

[7] Said F Mughabghab. *Atlas of Neutron Resonances: Resonance Parameters and Thermal Cross Sections. Z= 1-100*. Elsevier, 2006.

[8] Hans-Josef Allelein and Albert Ziegler. *Reactor technology. Physical and technical fundamentals. 2. new rev. ed.; Reaktortechnik. Physikalisch-technische Grundlagen*. 2013.

[9] Wolfgang Demtröder. *Experimentalphysik 4: Kern-, Teilchen-und Astrophysik*. Springer-Verlag, 2017.

[10] John R Lamarsh and Anthony John Baratta. *Introduction to nuclear engineering*. Vol. 3. Prentice hall Upper Saddle River, NJ, 2001.

[11] Munshi Golam Mustafa, Ulrich Mosel, and HW Schmitt. "Asymmetry in nuclear fission". In: *Physical Review C* 7.4 (1973), p. 1518.

[12] National Nuclear Data Center. *Chart Of Nuclides*. 2018. URL: https://www-nds.iaea.org/relnsd/vcharthtml/VChartHTML.html.

[13] Mario Villa. *Reaktorphysik*. TU Wien, 2008.

[14] International Atomic Energy Agency. *Operational and long-term shutdown reactors*. 2019. URL: https://pris.iaea.org/PRIS/worldstatistics/OperationalReactorsByType.aspx.

[15] Wikimedia Commons. *File:Boiling water reactor english.svg — Wikimedia Commons, the free media repository*. [Online; accessed 27-March-2019]. 2017. URL: https://pris.iaea.org/PRIS/WorldStatistics/OperationalReactorsByType.aspx.

[16] Wikimedia Commons. *File:KKW mit DWR.png — Wikimedia Commons, the free media repository*. [Online; accessed 27-March-2019]. 2016. URL: https://commons.wikimedia.org/w/index.php?title=File:KKW_mit_DWR.png&oldid=208106364.

[17] United States Nuclear Regulatory Commission. *Westinghouse AP1000 Design Control Document Rev. 19 - Reactor - Section 4.2 Fuel System Design*. 2011. URL: https://www.nrc.gov/docs/ML1117/ML11171A444.pdf.

[18] United States Nuclear Regulatory Commission. *Westinghouse AP1000 Design Control Document Rev. 19 - Reactor - Section 4.3 Nuclear Design*. 2011. URL: https://www.nrc.gov/docs/ML1117/ML11171A445.pdf.

[19] Mary Eagleson et al. *Concise encyclopedia chemistry*. Walter de Gruyter, 1994.

[20] United States Nuclear Regulatory Commission. *Westinghouse AP1000 Design Control Document Rev. 19 - Reactor Coolant System and Connected Systems - Section 5.3 Reactor Vessel*. 2011. URL: https://www.nrc.gov/docs/ML1117/ML11171A453.pdf.

[21] United States Nuclear Regulatory Commission. *Westinghouse AP1000 Reactor Internals Design Changes*. 2007. URL: https://www.nrc.gov/docs/ML0704/ML070460604.pdf.

[22] United States Nuclear Regulatory Commission. *Westinghouse AP1000 Design Control Document Rev. 19 - Reactor Coolant System and Connected Systems - Section 5.4 Component and Subsystem Design*. 2011. URL: https://www.nrc.gov/docs/ML1117/ML11171A454.pdf.

[23] United States Nuclear Regulatory Commission. *Westinghouse AP1000 Design Control Document Rev. 19 - Reactor Coolant System and Connected Systems - Section 5.1 Summary Description*. 2011. URL: https://www.nrc.gov/docs/ML1117/ML11171A450.pdf.

[24] Kostadin Ivanov. *NucE 521 Neutron Transport Theory*. Penn State College of Engineering. 2018. URL: https://www.engr.psu.edu/cde/courses/nuce521/nuce521_chapter1_reading.pdf.

[25] E.E. Lewis and W.F. Miller. *Computational methods of neutron transport*. Jan. 1984.

[26] X-5 Monte Carlo Team. *MCNP - A General Monte Carlo N-Particle Transport Code, Version 5; Volume I: Overview and Theory*. 2003. URL: https://laws.lanl.gov/vhosts/mcnp.lanl.gov/pdf_files/la-ur-03-1987.pdf.

[27] Muhammad Naveed Khan. "Shield Design Analysis of Pressurized Water Reactor Using Monte Carlo Computer Code MCBEND". MA thesis. Department of Nuclear Engineering Pakistan Institute of Engineering & Applied Sciences, 2015.

[28] Ralph G. Williams, Christopher J. Gesh, and Richard T. Pagh. *Compendium of Material Composition Data for Radiation Transport Modeling*. 2006. URL: https://www.pnnl.gov/main/publications/external/technical_reports/PNNL-15870.pdf.

[29] MatWeb LLC. *MatWeb Material Property Data*. 2018. URL: http://www.matweb.com/.

[30] Micro-Simulation Technology. *Personal Computer Transient Analyzer*. 2017. URL: http://www.microsimtech.com/pctran/.

[31] Fatin Nabilah Tajul Ariffin et al. "Effect of Boron Carbide addition on the physical, mechanical and microstructural properties of Portland cement concrete". In: *Journal of Applied Sciences* 11.22 (2011), pp. 3738–3743.